Naval Research Laboratory

Washington, DC 20375-5320

NRL/FR/7163--12-10,226

Modal Theory of Transverse Acoustic Coherence in Shallow Oceans

PETER C. MIGNEREY

Acoustic Signal Processing and Systems Branch
Acoustics Division

September 28, 2012

REPORT DOCUMENTATION PAGE

Form Approved
OMB No. 0704-0188

1. REPORT DATE *(DD-MM-YYYY)*	**2. REPORT TYPE**	**3. DATES COVERED** *(From - To)*
28-09-2012	Formal Report	Nov. 2008 – May 2012

4. TITLE AND SUBTITLE

Modal Theory of Transverse Acoustic Coherence in Shallow Oceans

5a. CONTRACT NUMBER

5b. GRANT NUMBER

5c. PROGRAM ELEMENT NUMBER
62435N

6. AUTHOR(S)

Peter C. Mignerey

5d. PROJECT NUMBER

5e. TASK NUMBER
UW-435-010

5f. WORK UNIT NUMBER
6044, 6539

7. PERFORMING ORGANIZATION NAME(S) AND ADDRESS(ES)

Naval Research Laboratory
Acoustics Division
4555 Overlook Avenue, SW
Washington, DC 20375-5320

8. PERFORMING ORGANIZATION REPORT NUMBER

NRL/FR/7163--12-10,226

9. SPONSORING / MONITORING AGENCY NAME(S) AND ADDRESS(ES)

Office of Naval Research
One Liberty Center
875 N. Randolph Street, Suite 1425
Arlington, VA 22203-1995

10. SPONSOR / MONITOR'S ACRONYM(S)

ONR

11. SPONSOR / MONITOR'S REPORT NUMBER(S)

12. DISTRIBUTION / AVAILABILITY STATEMENT

Approved for public release; distribution is unlimited.

13. SUPPLEMENTARY NOTES

14. ABSTRACT

The coherence of a shallow-water acoustic field transverse to the propagation path is represented using adiabatic normal modes, and path-integral theory is applied to fluctuations of mode amplitudes to obtain the coherence function. The problem is formulated in the horizontal plane where ray paths are nearly straight having no interaction with lateral boundaries, and requires the spectrum of environmental fluctuations that are provided by a shallow-water Garrett–Munk internal-wave model. The coherence function of the acoustic field is shown to depend on phase-structure functions of the normal modes. Environmental fluctuations with wavevectors transverse to the acoustic path were found to govern the structure functions. The impact of internal waves on coherence is proportional to the internal-wave energy, and is strongest for the lowest internal-wave modes in conjunction with those acoustic modes having maxima in the vicinity of high buoyancy. The transverse phase-structure function is found to behave like a sinc function, which provides the transition between limiting solutions for small and large hydrophone separations. Results show the coherence predicted by the theory decays too slowly with hydrophone separation to describe the observed ocean.

15. SUBJECT TERMS

Acoustic coherence
Normal modes
Path integral
Garrett–Munk spectrum

16. SECURITY CLASSIFICATION OF:			**17. LIMITATION OF ABSTRACT**	**18. NUMBER OF PAGES**	**19a. NAME OF RESPONSIBLE PERSON**
a. REPORT	**b. ABSTRACT**	**c. THIS PAGE**			Peter Mignerey
Unclassified	Unclassified	Unclassified	UU	42	**19b. TELEPHONE NUMBER** *(include area code)* 202-767-2230

Standard Form 298 (Rev. 8-98)
Prescribed by ANSI Std. Z39.18

CONTENTS

MODAL THEORY OF TRANSVERSE ACOUSTIC COHERENCE IN SHALLOW OCEANS

1. INTRODUCTION

Ocean-acoustic systems operating in continental-shelf regions must cope with dynamic sound-speed fields that are driven by oceanographic processes. In such environments, acoustic fields are known to fluctuate significantly, and it is clear from the physics of the problem that the acoustical fluctuations are governed by those of the underlying sound-speed field, which is affected by diverse oceanic processes including surface waves, internal waves, bubble clouds, fish schools, bottom topography, and sub-bottom geology. The present work is focused solely on the relationship between the internal-wave spectrum and acoustic coherence in shallow oceans.

Awareness of the impact of internal waves and tides on acoustic propagation in the ocean was attributed by Whitmarsh et al. [1] to work conducted during World War II. Whitmarsh et al. themselves compared acoustic scattering of 25 kHz pulses at 256 m range with theoretical predictions of Skudrzyk [2] that were based on spatial correlation functions and the focusing of sound by anomalous sound-speed patches. Their conclusions, valid for high-frequency propagation at short range, are that amplitude variance increases with range, independent of the sea state. Lee [3, 4] based his efforts on work done by Ufford that was also done during World War II and published afterward [5, 6]. Using ray-based numerical simulations, Lee [3] demonstrated that internal waves can cause an increase in acoustic intensity contrast in comparison with the absence of such waves. DeFerrari [7] conducted ray-based simulations of long-range deep-water acoustic propagation through internal tides and waves that demonstrated phase shifts among multipath arrivals are the underlying cause of temporal fluctuations in acoustic intensity.

Breaking with the ray-based work, much of it in the temporal domain, Flatté and Tappert [8] combined a parabolic-equation acoustic model with the Garrett–Munk internal-wave spectrum, in a study which demonstrated significant impact of internal waves on acoustic propagation in deep-water environments. Munk and Zachariasen [9] combined a geometric-optics approximation of the acoustic field with the Garrett–Munk spectrum to rigorously relate, for the first time, internal-wave and acoustical statistics, which compared well with data from two experiments. A good historical review of work in this area may be found in Flatté [10].

In ocean basins with a deep sound channel, the physical difficulties related to boundary interactions are somewhat less daunting than in shallow-water environments, which have multiple boundary reflections. Here, path-integral techniques were successfully adapted to the propagation of waves in random media by Dashen [11]. Using this approach, Esswein and Flatté rigorously related sound-speed fluctuations due to linear internal waves, to the spatial and temporal coherence of acoustic fields [12].

Path-integral theories continue to be refined and used today for deep-water work being done by the Acoustic Thermometry of Ocean Climate (ATOC) and North Pacific Acoustic Laboratory (NPAL) groups [13–15]. One significant finding of the ATOC effort [16] has been the experimental verification in deep

Manuscript approved August 12, 2012.

water of the path-integral prediction that the mutual-coherence function of the acoustic field with complex pressure $P(y_i)$ has the form

$$\langle P_1 P_2^* \rangle = \langle |P_1||P_2| \rangle \exp(-\tfrac{1}{2} D(y_1 - y_2)), \tag{1}$$

where the phase-structure function $D(y_1 - y_2)$ is the variance of stochastic phase differences between two points in the acoustic field, and $\langle |P_1||P_2| \rangle$ is the amplitude covariance. One objective of the present work is to determine whether this exponential form holds in shallow water.

A normal-mode approach to acoustical fluctuations has also received long-standing attention, with the general conclusion that mode coupling induced by internal-wave fluctuations plays an important role in both deep and shallow water. Such couplings were clearly illustrated by the parabolic equation simulations of Colosi and Flatté [17]. Although it is an important component of the problem that eventually needs attention, the inclusion of coupling leads to considerable complications that require numerical evaluation [18]. By neglecting mode coupling, the analysis can be completed analytically, thus providing physical insight into the relationship between acoustical and environmental fluctuations. In this spirit, the incorporation of coupled modes into the path-integral approach is not included in the present work.

With respect to shallow-water oceans, various other parts of the problem have received attention over the past fifteen years. Preisig and Duda illustrated the resonant interaction of acoustic waves as they pass through large, nonlinear internal waves [19–21]. Finette et al. [22] performed data-constrained numerical simulations of acoustic intensity fluctuations observed in the 1995 Shallow-Water Acoustics in a Random Medium (SWARM) experiment [23]. Using numerical simulations, Finette and Oba [24] discovered the phenomenon of horizontal refraction of acoustic waves propagating nearly parallel to nonlinear internal-wave crests. However, a quantitative prediction of the transverse mutual-coherence function remains elusive for shallow oceans. The present work represents a step in that direction.

As currently formulated, path-integral theory applies to the fluctuation of a single refracted Fermat path that does not interact with boundaries. Clearly this restriction poses difficulties for shallow-water acoustic propagation, which not only has multiple boundary interactions, but is in fact modal for the lowest frequencies. To circumvent this problem in the present work, the acoustic propagation problem is formulated using adiabatic normal modes, and path-integral theory is applied to the propagation of mode amplitudes in the horizontal plane where there are no boundary interactions — all paths are refracted.

In the present work, the acoustic field is separated into adiabatic normal modes where a parabolic approximation of the Helmholtz equation governs the propagation of mode amplitudes. Here the horizontal wavenumbers provide stochastic indices of refraction. The wavefunction satisfying the parabolic equation is then written as an integral over all paths between a source and receiver, and the second moment is obtained by multiplying and ensemble averaging the wavefunctions of two receivers separated in space. After application of the Markov approximation and the Wiener–Khintchine theorem, the resulting phase-structure function emerges as an integral over the spectrum of transverse horizontal wavenumbers. Perturbations in the wavenumbers are related to those of the sound speed using an eigenvalue perturbation method adopted from quantum mechanics. The potential sound-speed gradient is then used to express the perturbations as a linear combination of internal-wave modes. The final result expresses the desired phase-structure function as an integral over the transverse internal-wave spectrum, which must be either measured or modeled. A shallow-water version of the Garrett–Munk spectrum is then introduced to provide one possible model.

The remainder of this work begins in Ch. 2 with theoretical development that expresses the acoustic coherence function as a weighted sum over mode-amplitude coherence functions. In Ch. 3, path-integral theory is applied to fluctuations of the mode-amplitude coefficients to obtain an expression for the spectral representation of the phase-structure function. In Ch. 4, fluctuations in the acoustic horizontal wavenumbers are related to those of a linear internal-wave field. In Ch. 5, everything is pulled together to produce a set of numerical simulations that illustrate the properties of transverse coherence under this theory.

2. MODAL REPRESENTATION OF COHERENCE

2.1 Mutual-Coherence Function

In the works of Esswein and Flatté [12], Flatté et al. [25], and Flatté and Stoughton [26], the scattering strength is defined as

$$\Phi \equiv \left\langle \left(\int_0^{S_L} k(\vec{x}(s))\mu(\vec{x}(s))\mathrm{d}s \right)^2 \right\rangle, \tag{2}$$

and the phase-structure function is defined as

$$D(\vec{x}_1,\vec{x}_2) \equiv \left\langle \left(\int_0^{S_L} k(\vec{x}_1(s))\mu(\vec{x}_1(s))\mathrm{d}s - \int_0^{S_L} k(\vec{x}_2(s))\mu(\vec{x}_2(s))\mathrm{d}s \right)^2 \right\rangle, \tag{3}$$

where $k(\vec{x})$ is the unperturbed wavenumber of the background environment, $\mu(\vec{x})$ are stochastic perturbations to the index of refraction, $\vec{x}(s)$ are spatial coordinates of a ray path, s is arc length along the unperturbed ray, and S_L is the total arc length. Properties of the phase-structure function are discussed in these works.

In the limit of geometric optics [25], the total phase-fluctuation $\delta\phi$ accumulates along the propagation path,

$$\delta\phi = \int_0^{S_L} k(\vec{x}(s))\mu(\vec{x}(s))\mathrm{d}s. \tag{4}$$

Under these conditions the scattering strength becomes the variance of phase fluctuations $\Phi = \langle \delta\phi^2 \rangle$, and likewise, the phase-structure function becomes the variance of fluctuations in phase difference [13, 26], $D(\vec{x}_1,\vec{x}_2) = \left\langle (\delta\phi_1 - \delta\phi_2)^2 \right\rangle$. The structure function is nonnegative, and for large hydrophone separations it approaches twice the scattering strength, $\left\langle (\delta\phi_1 - \delta\phi_2)^2 \right\rangle \to 2\Phi$.

Under further assumptions of Gaussian statistics for the phase fluctuations, it has been shown [25] that the normalized covariance between two points of a complex stochastic field $P(\vec{x})$ may be expressed as an exponential of the phase-structure function,

$$\frac{\langle P(\vec{x}_1)P^*(\vec{x}_2)\rangle}{P_0(\vec{x}_1)P_0^*(\vec{x}_2)} = \exp\left[-\tfrac{1}{2}D(\vec{x}_1,\vec{x}_2)\right], \tag{5}$$

where P_0 is the field in the absence of fluctuations. This well-established equation has been derived using several different methods [10, 27]. Equation (5) can be derived under less restrictive conditions using the

path-integral approach [10, 11, 27]. In particular, Dashen [11] has shown that the only requirements for the validity of Eq. (5) are that the medium be isotropic and the narrow-angle parabolic approximation hold. Thus Gaussian statistics for the phase fluctuations are not strictly necessary. Colosi et al. [16] has shown that Eq. (5) may be expressed in terms of amplitude and phase correlations as

$$\langle P_1 P_2^* \rangle = \langle |P_1|\,|P_2| \rangle \exp\left[-\tfrac{1}{2} D(\vec{x}_1, \vec{x}_2)\right]. \tag{6}$$

Under conditions of statistical homogeneity [15], the mutual-coherence function $R_P(\Delta y)$ of the acoustic pressure $P(y)$ is defined by

$$R_P(\Delta y) \equiv \frac{\langle P(y) P^*(y+\Delta y) \rangle_{t,y}}{\left\langle |P(y)|^2 \right\rangle_{t,y}}, \tag{7}$$

where Δy is hydrophone separation transverse to the acoustic propagation path, the ensemble average is both over blocks of time assuming the ergodic hypothesis, and over the sub-diagonal elements of a Toeplitz cross-spectral density matrix. By combining Eqs. (6) and (7), the relationship between the mutual-coherence function and the phase-structure function is

$$R_P(\Delta y) = \frac{\langle |P(y)|\,|P(y+\Delta y)| \rangle_{t,y}}{\left\langle |P(y)|^2 \right\rangle_{t,y}} \exp\left[-\tfrac{1}{2} D(\Delta y)\right]. \tag{8}$$

To remove the amplitude correlation from measured acoustic data for comparison with the theory developed below, the complex hydrophone pressures P_i are normalized as $\tilde{P}_i \equiv P_i/|P_i|$. Thus the normalized mutual-coherence function is related to the phase-structure function by

$$\begin{aligned} \tilde{R}_P(\Delta y) &= \left\langle \tilde{P}(y) \tilde{P}^*(y+\Delta y) \right\rangle_{t,y} \\ &= \exp\left[-\tfrac{1}{2} D(\Delta y)\right]. \end{aligned} \tag{9}$$

Note, with this definition the reference coherence is $e^{-1/2} = 0.6$, where the coherence scale length L is defined to be $\Delta y = L$ such that $D = 1$.

By making a small-aperture approximation [12, 26, 27], the form of the phase-structure function was determined to obey a power law

$$D_P(\Delta y) = \left(\frac{\Delta y}{L}\right)^n, \tag{10}$$

where L is the transverse coherence length. The correct value to use for n is not clearly resolved in the literature. Cox [28] simply assumed $n = 1$ in his work that predates the path-integral approach, and found reasonable agreement with his data. Carey [29] reviewed various works that assumed $n = 1.0, 1.5, 2.0$, and then presented an array-signal-gain approach that is solvable for those three values. For observations of transverse coherence in the Strait of Korea, Carey et al. [30] used $n = 2.0$. Esswein and Flatté [12] evaluated $D_P(\Delta y)$ numerically but did not report an exponent. Dashen et al. [27] fit a phenomenological phase-correlation function with exponent $n = 1.5$ to Esswein's numerical results. This value was then adopted in

the follow-on works of Flatté and Stoughton [26] and Flatté and Rovner [14]. For deep-water data obtained in the Pacific, Andrew et al. [15] found good agreement between the observed mutual-coherence function, detailed numerical calculations using the technique of Flatté and Rovner [14], and a small-aperture empirical exponential with $n = 1.5$. Yet there are theoretical indications in Dashen [11] and in the results presented below that $n = 2.0$ for small separations of the path-integral solution. Whatever the correct value of n may be for small Δy, the exponential approximation must break down at large separations [26] where the power law vanishes, whereas the coherence decays to a constant value, $R_P(\Delta y) \to \exp(-\Phi)$.

2.2 Modal Expansion of Acoustic Field

The problem is formulated in cylindrical coordinates $\mathbf{u} \equiv (r, \theta, z)$ beginning with the frequency-domain Helmholtz equation

$$\frac{1}{r}\frac{\partial}{\partial r}\left(r\frac{\partial P}{\partial r}\right) + \frac{\partial^2 P}{r^2 \partial \theta^2} + \bar{\rho}(z)\frac{\partial}{\partial z}\left(\frac{1}{\bar{\rho}(z)}\frac{\partial P}{\partial z}\right) + k^2(\mathbf{u})P = -Q_s \frac{\delta(r)\delta(z-z_s)}{2\pi r}, \tag{11}$$

which describes the acoustic pressure $P(\mathbf{u})$ of a narrowband source with angular frequency $\omega = 2\pi f$ and wavenumber $k(\mathbf{u}) = \omega/c(\mathbf{u})$, where $c(\mathbf{u})$ is the sound speed, and $\bar{\rho}(z)$ is the mean density stratification. Here the source term takes the form $\delta(\mathbf{u}-\mathbf{u}_s) = \delta(r)\delta(z-z_s)/2\pi r$, with Q_s as the source strength. A separation of variables [31] then leads to an expansion of the acoustic pressure in terms of local modes, which vary over the horizontal plane [32–34],

$$P(r, \theta, z) = \sum_{m=1}^{M} A_m(r, \theta)\Psi_m(r, \theta; z). \tag{12}$$

The real eigenfunctions $\Psi_m(r, \theta; z)$ are normalized such that

$$\int_0^\infty \Psi_m(z)\Psi_n(z)/\bar{\rho}(z)\mathrm{d}z = \delta_{mn}, \tag{13}$$

and assumed to vary slowly over the horizontal plane (r, θ); but the complex mode amplitudes $A_m(r, \theta)$ vary much more rapidly due to fluctuations in the environment. Following Pierce [32], mode coupling is neglected.

With the separation of variables Eq. (12), the Helmholtz equation Eq. (11) splits into a Sturm–Liouville equation Eq. (14) for the eigenfunctions and the horizontal wavenumbers $k_m(r, \theta)$; and a two-dimensional Helmholtz equation Eq. (15) for the mode coefficients $A_m(r, \theta)$ in which the horizontal wavenumbers are effectively the index of refraction,

$$\bar{\rho}(z)\frac{\partial}{\partial z}\left(\frac{1}{\bar{\rho}(z)}\frac{\partial \Psi_m(r, \theta; z)}{\partial z}\right) + \left(k^2(r, \theta; z) - k_m^2(r, \theta)\right)\Psi_m(r, \theta; z) = 0, \quad \text{and} \tag{14}$$

$$\frac{1}{r}\frac{\partial}{\partial r}\left(r\frac{\partial A_m(r, \theta)}{\partial r}\right) + \frac{\partial^2 A_m(r, \theta)}{r^2 \partial \theta^2} + k_m^2(r, \theta)A_m(r, \theta) = -Q_s \frac{\delta(r)}{2\pi r}\Psi_m(0, 0; z_s). \tag{15}$$

The mode coefficients $A_m(r,\theta)$ are subject to stochastic perturbations due to sound-speed inhomogeneities and bottom irregularities. This follows from $k(r,\theta;z) = \omega/c(r,\theta;z)$, which makes $k_m(r,\theta)$ stochastic in Eq. (14), and $A_m(r,\theta)$ stochastic in Eq. (15). Unlike the eigenfunctions, these environmental perturbations are assumed to vary rapidly over the horizontal plane. Because normal-mode amplitudes propagate in the horizontal plane along independent paths through the ocean, they are affected by unrelated sound-speed fluctuations. This process causes statistical independence among the mode amplitudes.

For a horizontal line array oriented broadside toward an acoustic source, and with an aperture small compared to the source-receiver range, curvature of the acoustic field may be neglected, and the receiver range $r = x_o$ and depth z_o are constant. These assumptions allow a simplification of notation: $y \equiv x_o\theta$, $P(y) \equiv P(x_o,y,z_o)$, $A_m(y) \equiv A_m(x_o,y)$, and $\Psi_m(y) \equiv \Psi_m(x_o,y,z_o)$. Furthermore under these assumptions, eigenfunctions that vary slowly over the horizontal plane effectively remain constant across the array aperture, $\Psi_m(y) \equiv \Psi_m$, $\forall y$. The normal-mode expansion, Eq. (12), for the acoustic pressure field evaluated along a broadside horizontal array then becomes

$$P(y) = \sum_{m=1}^{M} A_m(y)\Psi_m. \tag{16}$$

2.3 Modal Expansion of Coherence Function

The normal-mode expansion of the horizontal coherence function follows from substituting Eq. (16) into Eq. (7),

$$R_P(\Delta y) = \frac{1}{\sigma_P^2} \sum_{m=1}^{M} \sum_{n=1}^{M} \langle A_m(y) A_n^*(y+\Delta y)\rangle_{t,y} \Psi_m \Psi_n, \tag{17}$$

where $\sigma_P^2 \equiv \langle |P(y)|^2 \rangle_{t,y}$ is the expected value of the acoustic field intensity. The mode amplitudes propagating along independent paths are affected by unrelated sound-speed fluctuations, hence statistical independence of the fluctuations make the cross-modal amplitude matrix diagonal, $\langle A_m(y) A_n^*(y+\Delta y)\rangle_{t,y} \approx 0$, $m \neq n$. The modal expansion of the cross-spectral density matrix Eq. (17) then becomes a single sum over the modes,

$$R_P(\Delta y) = \frac{1}{\sigma_P^2} \sum_{m=1}^{M} \langle A_m(y) A_m^*(y+\Delta y)\rangle_{t,y} \Psi_m^2. \tag{18}$$

Because the full acoustic field is homogeneous, each cross-modal amplitude matrix is also homogeneous with the same form as Eq. (7),

$$R_{A_m}(\Delta y) \equiv \frac{\langle A_m(y) A_m^*(y+\Delta y)\rangle_{t,y}}{\sigma_{A_m}^2}, \tag{19}$$

where $\sigma_{A_m}^2 \equiv \langle A_m(y)^2 \rangle_{t,y}$ is the expected intensity of each normal mode, and $R_{A_m}(\Delta y)$ is the mutual-coherence function of each mode amplitude.

As with the total acoustic field, the modal coherence functions may be separated into an amplitude correlation and a modal phase-structure function $D_m(\Delta y)$ with the associated normalized form

$$\begin{aligned} \tilde{R}_{A_m}(\Delta y) &= \left\langle \tilde{A}_m(y)\tilde{A}_m^*(y+\Delta y)\right\rangle_{t,y} \\ &= \exp\left[-\tfrac{1}{2}D_m(\Delta y)\right], \end{aligned} \tag{20}$$

where $\tilde{A}_m(y) \equiv A_m(y)/|A_m(y)|$. The theory developed below relates $D_m(\Delta y)$ to the internal-wave spectrum.

The normal-mode expansion of the horizontal coherence function is then

$$R_P(\Delta y) = \sum_{m=1}^{M} \frac{\sigma_{A_m}^2 \Psi_m^2}{\sigma_P^2} R_{A_m}(\Delta y), \tag{21}$$

where $\sigma_P^2 = \sum_{m=1}^{M} \sigma_{A_m}^2 \Psi_m^2$ shows the field power is the total power in the modes evaluated at the array depth. Here the total power is a normalization constant that enforces $R_P(0) = 1$.

The functional form of Eq. (21) is generally true for any statistical process that is a sum of independent zero-mean subprocesses each with variance σ_m^2. A similar result was found by Shifrin [35] using very general statistical arguments for radar-antenna field coherence. Similarly, for an acoustic field that is more appropriately represented by a superposition of rays, the horizontal coherence comprises a weighted sum of functions, each belonging to a ray that connects the source and receiver.

In the following sections a path-integral approach is used in conjunction with the Markov approximation and a spatial spectrum for linear internal waves to obtain an expression for $R_{A_m}(\Delta y)$.

3. MUTUAL COHERENCE OF MODE AMPLITUDES

3.1 Path Integral Representation of Modal Coherence

To obtain a path-integral expression for the horizontal coherence, the wave equation, Eq. (15), for the mode amplitudes is converted to Cartesian form. Let $x \equiv r$, the cross-range position be $y \equiv r\theta$, and drop the explicit dependence on horizontal position, $(r,\theta) \to (x,y)$, from the notation for A_m. In a far-field limit the transverse array aperture is much shorter than the range, i.e., $y \ll x_o$, and θ is small enough that wavefront curvature may be neglected.

Next a coordinate transformation is introduced that renders the problem Cartesian:

$$\hat{A}_m \equiv r^{-1/2} A_m, \tag{22}$$

$$\kappa_m^2 \equiv k_m^2 + 1/(2r)^2. \tag{23}$$

Henceforth the term horizontal wavenumber refers to the reduced wavenumber κ_m defined by Eq. (23).

Clearly this approximation breaks down where $r < 1/2k_m$. For the lowest acoustic modes associated with large k_m, breakdown occurs near the source. The path-integral solution presented below is then valid

from a few wavelengths beyond the source, through the ocean fluctuations to the receiver. For the highest modes that are near cutoff where $k_m \to 0$, the path-integral solution breaks down over the entire range.

Thus $k_m \approx \kappa_m$ in the remainder of this work. With this change of spatial coordinates and dependent variables, it can be shown that the homogeneous part of Eq. (15) reduces to the Cartesian form

$$\frac{\partial^2 \hat{A}_m}{\partial x^2} + \frac{\partial^2 \hat{A}_m}{\partial y^2} + \kappa_m^2(x,y)\hat{A}_m = 0. \tag{24}$$

Following Flatté [10] and Dashen et al. [27], let the perturbations of the horizontal wavenumber have the form

$$\kappa_m(x,y) = \bar{\kappa}_m \left(1 + u_m(x,y) + \mu_m(x,y)\right), \tag{25}$$

where $\bar{\kappa}_m \equiv \langle \kappa_m(x,y) \rangle_{x,y}$ is the mean horizontal wavenumber over the entire region between the source and receiver; $u_m(x,y)$ accommodates the coordinate transformation and describes a wavenumber "profile" that varies slowly over the horizontal plane, e.g., a gradient induced by propagation on a slope; and $\mu_m(x,y)$ are the random fluctuations that cause statistical variability in the acoustic field. $\bar{\kappa}_m$ is a dimensional scale factor and both u_m and μ_m are nondimensional. An important assumption here is that both the deterministic perturbation $u_m \ll 1$ and stochastic fluctuation $\mu_m \ll 1$ are small.

For the propagation of mode amplitudes in the horizontal plane, the dominant ray is nearly a straight path from source to receiver. Unlike propagation problems in the vertical plane, there are no multiple paths here except near caustics that form at mode cutoff for upslope configurations. Thus, it is reasonable to look for solutions of the form

$$\hat{A}_m(x,y) \equiv \psi_m(x,y) \exp\left(i\bar{\kappa}_m x\right). \tag{26}$$

In the small-angle parabolic approximation of Eq. (24), the $\partial^2 \psi_m / \partial x^2 \approx 0$ term is ignored, as are the quadratic wavenumber perturbations u_m^2, μ_m^2, and $u_m \mu_m$, thus producing

$$2i\bar{\kappa}_m \frac{\partial \psi_m}{\partial x} = -\frac{\partial^2 \psi_m}{\partial y^2} - 2\bar{\kappa}_m^2 \left(u_m(x,y) + \mu_m(x,y)\right) \psi_m. \tag{27}$$

(Also, a pair of low-order $\bar{\kappa}_m^2 \psi_m$ terms of opposite sign cancel.) As Tatarskii [36, p. 375] notes, the parabolic approximation is valid for small wavelengths where both $\lambda_m \ll l_e$ and $\lambda_m^3 x_o \ll l_e^4$. Here $\lambda_m = 2\pi/\bar{\kappa}_m$ is the horizontal wavelength of each mode; l_e is the scale length of environmental fluctuations; and x_o is the propagation range. These criteria clearly break down as $\bar{\kappa}_m \to 0$, which occurs for high-order modes near cutoff.

The path-integral solution to Eq. (27) is given by Flatté [10], Dashen [11], Esswein and Flatté [12], Flatté et al. [25], and Dashen et al. [27]:

$$\psi_m(x_o, Y) = (i/4\bar{\kappa}_m)^{1/2} \int \mathrm{D}p \exp\left\{ i\bar{\kappa}_m \int_0^{x_o} \left[U_m(x, y_p(x)) + \mu_m(x, y_p(x))\right] \mathrm{d}x \right\}, \tag{28}$$

$$U_m(x,y_p(x)) \equiv \frac{1}{2}\left(\frac{\partial y_p(x)}{\partial x}\right)^2 + u_m(x,y_p(x)), \tag{29}$$

where the subscript p denotes the path and $\int \mathrm{D}p$ indicates integration over all possible paths. In the above integral, all paths begin at the origin and terminate at the same point, $Y \equiv y_p(x_o)$, $\forall p$. Here $U_m(x,y_p(x))$ provides the solution in the absence of environmental fluctuations, while $\mu_m(x,y_p(x))$ introduces contributions from the fluctuations.

Dashen [11] and Dashen et al. [27] have demonstrated that the second moment of Eq. (28) may be written as an exponential of the phase-structure function,

$$\frac{\left\langle \psi_m(x_o,Y_\alpha)\psi_m^*(x_o,Y_\beta)\right\rangle_e}{\left\langle |\psi_m(x_o,0)|^2\right\rangle_e} = \exp\left[-\tfrac{1}{2}D_m(Y_\alpha,Y_\beta)\right], \tag{30}$$

where the path-integral solution for the structure function is

$$D_m(Y_\alpha,Y_\beta) = \bar{\kappa}_m^2 \left\langle \left(\int_0^{x_o} \mu_m(x_1,y_\alpha(x_1))\mathrm{d}x_1 - \int_0^{x_o} \mu_m(x_2,y_\beta(x_2))\mathrm{d}x_2\right)^2 \right\rangle_e . \tag{31}$$

The points $Y_\alpha \equiv y_\alpha(x_o)$ and $Y_\beta \equiv y_\beta(x_o)$ are the terminal transverse coordinates of two nearby principal rays α and β propagating through the *unperturbed* environment. The geometry of the principal rays and the coordinate system describing them is shown in Fig. 1. The expectation is taken over an ensemble of homogeneous stochastic environments e, thus $\left\langle |\psi_m(x,y)|^2\right\rangle_e = \left\langle |\psi_m|^2\right\rangle_e$ for all x,y. Also, use was made of the identity $\langle \exp(i\alpha)\rangle = \exp(-\frac{1}{2}\langle\alpha^2\rangle)$, which is valid for Gaussian random variables that result when the central-limit theorem is applied to $\alpha \equiv \int \mu_m(x)\mathrm{d}x$, even for non-Gaussian $\mu_m(x)$.

It must be emphasized here that Eq. (31) is derived from a double path integral obtained by integrating solutions to the parabolic equation over *all possible paths* between a source and two receivers (α and β). These paths through a stochastic environment fluctuate about two deterministic principal rays from the source to the pair of receivers. The principal rays are defined within the unperturbed environment, and diverge approximately linearly with range as discussed in Sec. 3.3. From the integrals of the index of refraction over range in Eq. (31), the phase structure is seen to arise from the expected value of stochastic differences in path length, and has the same form as Eq. (3) with a constant wavenumber.

These results for mutual coherence are valid regardless of scattering strength up until the parabolic approximation breaks down, and are not based on a stationary phase approximation through the fluctuations [27]. In the path-integral formulation of mutual coherence, global statistical properties reduce the integration over all possible paths to an integration over a single mean path [11]. The conditions of validity for Eqs. (30) and (31) are rigorously demonstrated in Appendix A of Ref. 11. The main result is that for an isotropic homogeneous medium, Eq. (30) is valid when the parabolic approximation is valid. The path-integral solution is very general [11, 27]. The assumptions are the parabolic approximation, homogeneity of environmental fluctuations in the transverse direction, and the existence of a *single* principal ray arriving at each receiver. Thus, these results are not valid in a multipath environment, such as shallow-water acoustic propagation in a vertical plane.

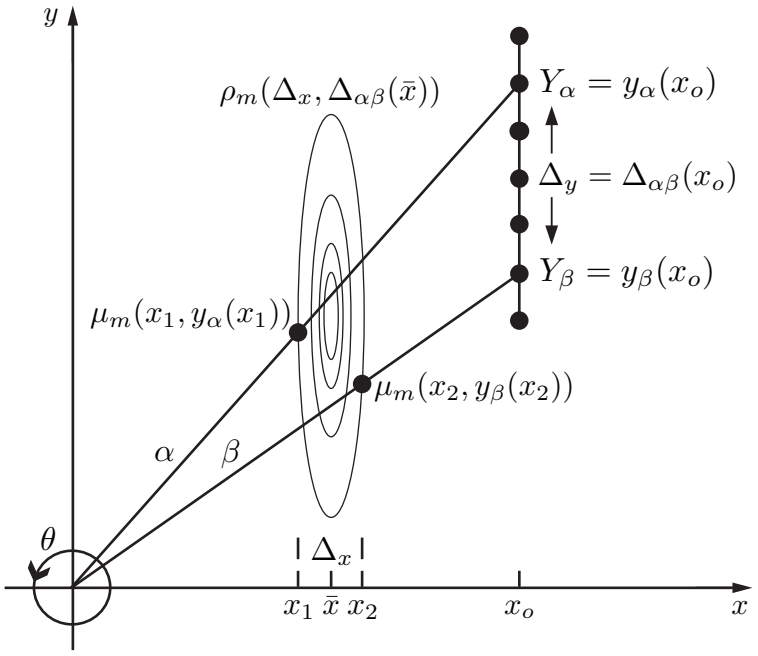

Fig. 1 — Geometry of two principal rays α and β propagating in the horizontal plane (x,y). The acoustic source is located at the origin, and the transverse receiver array represented by the vertical line of dots is located at range x_o. The nested ellipses represent the two-point correlation function, $\rho_m(\Delta_x,\Delta_{\alpha\beta}) = \langle \mu_m(x_1,y_\alpha)\mu_m(x_2,y_\beta)\rangle$, of fluctuations in the horizontal acoustic wavenumber $\mu_m(x,y)$.

For our problem of mode amplitudes propagating in a horizontal plane without lateral boundaries, the assumptions required by path-integral theory are reasonable. Here there are no lateral boundaries to cause multiple paths. Mode amplitudes propagating in the horizontal plane governed by Eq. (24) follow benign paths that diverge slowly, except up a slope near mode cutoff where caustics form [33, 37, 38]. It remains now to determine precisely the decay rate for homogeneous isotropic shallow-water environments.

3.2 Markov Approximation of Phase-Structure Function

Following Esswein and Flatté [12], the phase-structure function Eq. (31) is expressed using a weak form of the Markov approximation. Unlike stratified propagation problems formulated in the vertical plane, here there is no anisotropy to contend with, which simplifies the final results.

Equation (31) is insensitive to interchanging the two paths, and they may be combined when the square is expanded,

$$D_m(Y_\alpha,Y_\beta) = 2\bar{\kappa}_m^2 \int_0^{x_o}\int_0^{x_o} \rho_m(x_1,x_2;y_\alpha(x_1),y_\alpha(x_2)) - \rho_m(x_1,x_2;y_\alpha(x_1),y_\beta(x_2))\mathrm{d}x_1\mathrm{d}x_2, \tag{32}$$

where the two-point correlation function of the environment between principal rays α and β is

$$\rho_m(x_1,x_2;y_\alpha(x_1),y_\beta(x_2)) \equiv \left\langle \mu_m(x_1,y_\alpha(x_1))\mu_m(x_2,y_\beta(x_2))\right\rangle_e . \tag{33}$$

Transverse homogeneity was assumed in the derivation of Eqs. (30) and (31), and here homogeneity in range is assumed as well:

$$\rho_m(x_1,x_2;y_\alpha(x_1),y_\beta(x_2)) = \rho_m(x_2-x_1,y_\beta(x_2)-y_\alpha(x_1)). \tag{34}$$

Additionally, the range variables are changed to a range difference and a mean range: $\Delta_x \equiv x_2 - x_1$, $\bar{x} \equiv (x_1+x_2)/2$; with associated changes in the cross-range direction: $\Delta_y \equiv \Delta_{\alpha\beta}(x_o)$, $\Delta_{\alpha\beta}(\bar{x}) \equiv y_\beta(\bar{x}) - y_\alpha(\bar{x})$. Again, see Fig. 1 for a sketch of the geometry.

Now the Markov approximation is made. Because $\rho_m(\Delta_x,\Delta_{\alpha\beta}(\bar{x}))$ is compact around $\Delta_x = 0$, the correlation function has support in range only where $x_1 \sim x_2 \sim \bar{x}$, and is negligible elsewhere. Hence, Esswein and Flatté [12] justify the approximation

$$\rho_m(x_2-x_1,y_\beta(x_2)-y_\alpha(x_1)) \approx \rho_m(\Delta_x,\Delta_{\alpha\beta}(\bar{x})). \tag{35}$$

Compactness also justifies extension of the integration limits,

$$\int_0^{x_o} \rho_m(\Delta_x,\Delta_{\alpha\beta}(\bar{x}))\mathrm{d}\Delta_x \int_{-\infty}^{\infty} \rho_m(\Delta_x,\Delta_{\alpha\beta}(\bar{x}))\mathrm{d}\Delta_x. \tag{36}$$

In the strong Markov approximation the correlation in range is infinitesimal,

$$\rho_m(\Delta_x,\Delta_{\alpha\beta}(\bar{x})) \approx \delta(\Delta_x)\rho_m(\Delta_{\alpha\beta}(\bar{x})). \tag{37}$$

With the weak Markov approximation, the correlation in range remains finite. With these homogeneity and compactness assumptions, the phase-structure function, Eq. (32), becomes

$$D_m(\Delta_y) = 2\bar{\kappa}_m^2 \int_0^{x_o} \int_{-\infty}^{\infty} \rho_m(\Delta_x,0) - \rho_m(\Delta_x,\Delta_{\alpha\beta}(\bar{x}))\mathrm{d}\Delta_x\mathrm{d}\bar{x}. \tag{38}$$

The Markov approximation breaks down near turning points where the ray curvature is large in comparison with the correlation length of environmental fluctuations. This difficulty does not occur for the shallow-water propagation of normal-mode amplitudes in the horizontal plane. Here, the problem of large ray curvature occurs only on slopes in the vicinity of caustics near mode cutoff.

3.3 Spectral Representation of Phase-Structure Function

The stochastic acoustic horizontal-wavenumber fluctuations $\mu_m(x,y)$ are zero mean by definition, and in the development of the phase-structure function the process was also assumed homogeneous. It is thus reasonable to assume that the fluctuations belong to a stationary stochastic process. Under these conditions the correlation function $\rho_m(\Delta_x,\Delta_{\alpha\beta}(\bar{x}))$ may be represented in spectral form via the Wiener–Khintchine theorem [39],

$$\rho_m(\Delta_x,\Delta_{\alpha\beta}(\bar{x})) = \int_{-\infty}^{\infty}\int_{-\infty}^{\infty} S_m(\gamma_x,\gamma_y) e^{\left[i\left(\gamma_x\Delta_x+\gamma_y\Delta_{\alpha\beta}(\bar{x})\right)\right]}\mathrm{d}\gamma_x\mathrm{d}\gamma_y, \tag{39}$$

where γ_x and γ_y are the horizontal wavenumbers in the range and transverse directions for the power spectrum $S_m(\gamma_x,\gamma_y)$ of the acoustic horizontal-wavenumber fluctuations. Note there are two very different types of

horizontal wavenumber in this problem. The horizontal wavenumbers of the acoustic field, κ_m, act as indices of refraction governing the horizontal propagation of the normal-mode amplitudes, whether the propagation be deterministic or stochastic. When the propagation is stochastic, fluctuations of this index, μ_m, also have a power spectrum S with horizontal wavenumbers denoted by γ_x and γ_y.

The integrals that compose the phase-structure function Eq. (38) are represented in spectral form as

$$\int_{-\infty}^{\infty} \rho_m(\Delta_x, \Delta_{\alpha\beta}(\bar{x}))\mathrm{d}\Delta_x = 2\pi \int_{-\infty}^{\infty}\int_{-\infty}^{\infty} S_m(\gamma_x,\gamma_y)\,\delta(\gamma_x) e^{\left(i\gamma_y\Delta_{\alpha\beta}(\bar{x})\right)}\mathrm{d}\gamma_x\mathrm{d}\gamma_y, \tag{40}$$

after substituting $\int_{-\infty}^{\infty} e^{i(\gamma_x\Delta_x)}\mathrm{d}\Delta_x = 2\pi\,\delta(\gamma_x)$. Now assume horizontal isotropy by letting $\gamma_x = \gamma_h\cos(\theta)$ and $\gamma_y = \gamma_h\sin(\theta)$, and note that with this change of coordinates $\delta(\gamma_x) \to \delta(\gamma_h\cos(\theta))$ and $\mathrm{d}\gamma_x\mathrm{d}\gamma_y \to \gamma_h\mathrm{d}\gamma_h\mathrm{d}\theta$ where the delta function is nonzero for $\gamma_h > 0$ when $\theta = 2n\pi \pm \pi/2$, then the correlation function becomes

$$\int_{-\infty}^{\infty} \rho_m(\Delta_x, \Delta_{\alpha\beta}(\bar{x}))\mathrm{d}\Delta_x = 2\pi \int_{0}^{\infty} S_m(\gamma_h)\left[e^{\left(+i\gamma_h\Delta_{\alpha\beta}(\bar{x})\right)} + e^{\left(-i\gamma_h\Delta_{\alpha\beta}(\bar{x})\right)}\right]\gamma_h\mathrm{d}\gamma_h, \tag{41}$$

and likewise when $\Delta_{\alpha\beta} = 0$,

$$\int_{-\infty}^{\infty} \rho_m(\Delta_x, 0)\mathrm{d}\Delta_x = 4\pi \int_{0}^{\infty} S_m(\gamma_h)\,\gamma_h\mathrm{d}\gamma_h. \tag{42}$$

Because of the properties of $\delta(\gamma_h\cos(\theta))$, $\gamma_x = 0$ and $\gamma_y = \pm\gamma_h$, thus showing that Eqs. (41) and (42) depend solely on the transverse part of the spectrum. From this it is apparent that only environmental fluctuations with wavevectors normal to the main acoustic path contribute to the transverse coherence. Contributions from fluctuations with wavevectors parallel to the acoustic path average out to zero. The spectral representation of the phase-structure function, Eq. (38), then becomes

$$D_m(\Delta_y) = 4\pi\bar{\kappa}_m^2 \int_0^{x_o}\int_0^{\infty} S_m(\gamma_h)\left[2 - \left[e^{\left(+i\gamma_h\Delta_{\alpha\beta}(\bar{x})\right)} + e^{\left(-i\gamma_h\Delta_{\alpha\beta}(\bar{x})\right)}\right]\right]\gamma_h\mathrm{d}\gamma_h\mathrm{d}\bar{x}. \tag{43}$$

To evaluate the integral over range $\bar{x}$, make the approximation that two nearby principal rays α and β diverge approximately linearly, $\Delta_{\alpha\beta}(\bar{x}) \approx \Delta_y\bar{x}/x_o$, as they propagate in the horizontal plane of the *unperturbed* environment. This approximation becomes exact for a constant-depth environment with uniform sound speed. Even when the rays curve weakly on a slope far from caustics, their relative divergence remains approximately linear in range. With this approximation the integral may be evaluated,

$$\int_0^{x_o} e^{\left(i\gamma_h\Delta_{\alpha\beta}(\bar{x})\right)}\mathrm{d}\bar{x} = (x_o/i\gamma_h\Delta_y)\left[e^{(i\gamma_h\Delta_y)} - 1\right], \tag{44}$$

and the phase-structure function becomes

$$\begin{aligned} D_m(\Delta_y) &= 4\pi x_o\bar{\kappa}_m^2 \int_0^{\infty} S_m(\gamma_h)\left[2 - \frac{e^{(i\gamma_h\Delta_y)} - e^{(-i\gamma_h\Delta_y)}}{i\gamma_h\Delta_y}\right]\gamma_h\mathrm{d}\gamma_h & (45)\\ &= 8\pi x_o\bar{\kappa}_m^2 \int_0^{\infty} S_m(\gamma_h)\left[1 - \mathrm{sinc}\left(\gamma_h\Delta_y\right)\right]\gamma_h\mathrm{d}\gamma_h. & (46) \end{aligned}$$

It must be emphasized here that the sinc function arises from an *integral over range* of phase-difference fluctuations between two principal rays, which happen to diverge linearly. It has nothing to do with restricting integration over all possible paths to a finite transverse region. Integration over all possible paths was done properly in Sec. 3.1.

The unknown spectral weighting $S_m(\gamma_h)$ makes it impossible to say much about the integral except for limiting cases. A power-series expansion of the sinc function for small Δ_y has quadratic behavior,

$$1 - \mathrm{sinc}(\gamma_h \Delta_y) \approx (\gamma_h \Delta_y)^2/6 - \mathscr{O}(\gamma_h \Delta_y)^4. \tag{47}$$

Conversely in the opposite limit $\Delta_y \to \infty$, the sinc function decays as the phase-structure function approaches the spectral form of the modal-scattering-strength parameter

$$D_m(\infty) = 8\pi x_o \bar{\kappa}_m^2 \int_0^\infty S_m(\gamma_h)\, \gamma_h \mathrm{d}\gamma_h, \tag{48}$$

where the integral is the total power in the horizontal-wavenumber spectrum.

The spectrum $S_m(\gamma_h)$ required by the phase-structure function can be obtained from a known correlation function $\rho_m(\Delta_x, \Delta_y)$. Because the internal-wave displacement fluctuations are assumed homogeneous and isotropic, the correlation function may be evaluated at any point in the ocean along any orientation. Thus it is sufficient to evaluate Eq. (41) at $\bar{x} = x_o$, where $\Delta_{\alpha\beta}(\bar{x}) = \Delta_y$, and solve for $S_m(\gamma_h)$. Equation (41) may then be rewritten as

$$\int_{-\infty}^{\infty} \rho_m(\Delta_x, \Delta_y) \mathrm{d}\Delta_x = 2\pi \int_{-\infty}^{\infty} S_m(\gamma_h) e^{i\gamma_h \Delta_y} |\gamma_h| \mathrm{d}\gamma_h, \tag{49}$$

where symmetry of the power spectrum $S_m(\gamma_h)$ has been exploited to combine the two halves of the integral. Equation (49) is then Fourier transformed to obtain

$$S_m(\gamma_h) = \frac{1}{2\pi|\gamma_h|} \int_{-\infty}^{\infty} \int_{-\infty}^{\infty} \rho_m(\Delta_x, \Delta_y) e^{-i\gamma_h \Delta_y} \mathrm{d}\Delta_x \mathrm{d}\Delta_y. \tag{50}$$

To make progress, either the spectrum or the correlation function must be connected to the underlying environmental fluctuations by direct experimental measurement, or by theoretical analysis of an internal-wave model. The latter approach is pursued in the following sections.

The appropriate fluctuation spectrum for shallow oceans is neither well established nor universal. Contributory processes that induce randomness include the thermohaline microstructure, linear and nonlinear internal waves, bottom impedance, bottom roughness, and surface waves [40]. These processes are site dependent and, excepting bottom properties, influenced by the seasonal stratification, tidal cycle, and weather. To proceed, the theoretical analysis of horizontal coherence must be restricted to a specific environment. Among the above processes, shallow-water environments often show evidence for the impact of internal waves, the process that will be pursued here.

4. ACOUSTIC AND INTERNAL-WAVE SPECTRA

In this section, a relationship between fluctuations in the acoustic horizontal wavenumbers and those of the internal-wave spectrum is obtained based on a perturbation expansion of the Helmholtz equation, in which the wavenumbers are linearized for small perturbations of the sound speed field. The sound-speed fluctuations themselves are related to internal-wave displacements using the potential sound-speed gradient and linear internal-wave modes as basis functions. Correlation functions are formed by taking the expected value of fluctuation products, and Eq. (50) is used to obtain the spectral relationship. Finally, a Garrett–Munk spectrum modified for shallow water is used for the transverse spatial spectrum of the internal waves.

4.1 Sound-Speed Perturbations

In App. A, a general solution is obtained for the relationship between stochastic fluctuations in the eigenvalues of the Helmholtz equation and those of the sound-speed field. For the acoustics problem under consideration, the solution for the eigenvalue fluctuations given by Eq. (A15) has the form

$$\mu_m(x,y) = \frac{\bar{k}^2}{\bar{\kappa}_m^2} \int_0^{z_o} \nu(x,y;z) \bar{\Psi}_m^2(z) / \bar{\rho}(z) \mathrm{d}z. \tag{51}$$

Equation (51) asserts that fluctuations in the horizontal wavenumber are approximately proportional in an integral sense to fluctuations in the total acoustic wavenumber. The stochastic sound-speed perturbations $\nu(x,y;z)$ required by Eq. (51) are obtained from internal-wave displacements. In Sec. 4.3 below, Eq. (51) is squared and an expected value taken to obtain ρ_m, which is required by Eq. (33) for use in Eq. (50).

4.2 Internal-Wave Displacements

In a stratified ocean, the sound-speed fluctuations within the water column are dominated by linear internal-wave displacements [9, 41]. Under these conditions the sound-speed gradient $\partial c/\partial z = \partial_p c/\partial z + \partial_a c/\partial z$ is the sum of an adiabatic gradient ∂_a and a potential gradient ∂_p, where only vertical fluctuations within the potential gradient contribute to the sound-speed fluctuations [8, 42, 43]. A relationship between vertical displacements and sound-speed fluctuations is then obtained by equating first-order terms from the Taylor-series expansion of $c(z)$ with similar terms from the sound-speed perturbation expansion $c(z) = \bar{c}\,(1 - v(z) - \nu(z))$ to obtain

$$\nu(x,y;z) = -\frac{1}{\bar{c}} \frac{\partial_p c}{\partial z}(x,y;z) \zeta(x,y;z). \tag{52}$$

Following Flatté and Tappert [8], Gill [44], and Tielbürger et al. [45], the vertical displacements of the water column, ζ, are expanded as a sum of J linear internal-wave modes W_j, with complex mode amplitudes g_j,

$$\zeta(x,y;z,t) = \sum_{j=1}^{N} \int_0^{\infty} \int_0^{2\pi} g_j(\gamma_h,\theta) W_j(x,y;z,\gamma_h) e^{i\left[x\gamma_h\cos(\theta) + y\gamma_h\sin(\theta) - \omega_j t\right]} \mathrm{d}\theta\, \gamma_h \mathrm{d}\gamma_h, \tag{53}$$

where (x,y) are horizontal coordinates, t is time, and z is depth with the free surface at $z = 0$ and ocean bottom at $z = z_o$. The associated Cartesian wavenumbers are $\gamma_x = \gamma_h \cos(\theta)$ and $\gamma_y = \gamma_h \sin(\theta)$, which in

cylindrical coordinates in wavenumber space are written in terms of the total horizontal wavenumber γ_h and an angle in the horizontal plane θ.

The vertical oscillation frequencies $\omega_j(\gamma_h)$ and internal-wave mode functions $W_j(z,\gamma_h)$ are the parameterized eigenvalues (dispersion relation) and eigenfunctions of a well-known Sturm–Liouville problem [25, 44, 46–49] for the unperturbed, stratified, spatially homogeneous, mean environment. The $W_j(z,\gamma_h)$ are deterministic mode functions, with associated buoyancy frequency $N(z)$, of a stratified spatially homogeneous mean environment that satisfies

$$\frac{\partial^2 W_j(z,\gamma_h)}{\partial z^2} + \gamma_h^2 \left[\frac{N^2(z) - \omega_j^2}{\omega_j^2 - f_c^2} \right] W_j(z,\gamma_h) = 0, \tag{54}$$

such that $W_j(0) = 0$, $W_j(z_o) = 0$, and with a normalization that ignores the Earth's rotation [25],

$$\int_0^{z_o} N^2(z) W_i(z,\gamma_h) W_j(z,\gamma_h) \mathrm{d}z = \delta_{ij}, \quad \forall \gamma_h, \tag{55}$$

where δ_{ij} is the Kronecker delta. Here $f_c = 2\Omega\sin(\phi)$ is the local Coriolis frequency, $\Omega = 7.292\ 10^{-5}\,\mathrm{rad/s}$ is the Earth's rotation rate, and ϕ is the latitude.

The mode coefficients $g_j(\gamma_h,\theta)$ are samples of stochastic, zero-mean, complex amplitudes [17, 25] drawn from a distribution having a second moment $< g_j g_j^* >_e$ that is isotropic and homogeneous. It is important to include the angular dependence in $g_j(\gamma_h,\theta)$ because internal waves arriving from different directions are generated by unrelated physical processes.

Unless the bottom slope or horizontal density gradient is large, e.g., in the vicinity of a shelf-break front, the unperturbed seasonal stratification is nearly uniform over a horizontal plane that spans just a few tens of kilometers. Under these conditions there is no coupling between internal-wave modes, and the associated mode functions are approximately independent of horizontal position, $W_j(x,y;z,\gamma_h) \approx W_j(z,\gamma_h)$, $N(x,y;z) \approx N(z)$, and $\partial_p c(x,y;z)/\partial z \approx \partial_p c(z)/\partial z$.

With these approximations, Eqs. (51) – (53) become

$$\mu_m(x,y;t) = \frac{-\bar{k}^2}{\bar{\kappa}_m^2} \sum_{j=1}^{N} \int_0^{\infty} \mathscr{N}_{m,j}(\gamma_h) \int_0^{2\pi} g_j(\gamma_h,\theta) e^{i\left[x\gamma_h\cos(\theta) + y\gamma_h\sin(\theta) - \omega_j t\right]} \mathrm{d}\theta\, \gamma_h \mathrm{d}\gamma_h, \quad \text{and} \tag{56}$$

$$\mathscr{N}_{m,j}(\gamma_h) \equiv \int_0^{z_o} \frac{1}{\bar{c}} \frac{\partial_p c}{\partial z}(z) \bar{\Psi}_m^2(z) W_j(z,\gamma_h) \mathrm{d}z. \tag{57}$$

The importance of Eq. (57) is that it weights most heavily those internal-wave displacements at depths where the potential sound-speed gradient is large, i.e., within the thermocline, and deemphasizes high-order internal modes that oscillate rapidly in that part of the integral. The impact of this process on any particular acoustic mode depends on how the shape of the acoustic mode function aligns with the internal-wave excitation. Acoustic modes with maxima in the vicinity of large potential sound-speed gradients suffer more severe transverse coherence loss than modes with a null near the gradient.

4.3 Internal-Wave Correlation Function

A relationship between the acoustic correlation function and the internal-wave spectrum is obtained by substituting Eq. (56) into Eq. (33):

$$\rho_m(\Delta_x,\Delta_y) = \left(\frac{\bar{k}^2}{\bar{\kappa}_m^2}\right)^2 \sum_{j_1=1}^{N}\sum_{j_2=1}^{N}\int_0^\infty\int_0^\infty \mathscr{N}_{m,j_1}(\gamma_{h_1})\mathscr{N}_{m,j_2}(\gamma_{h_2})\int_0^{2\pi}\int_0^{2\pi}\left\langle g_{j_1}(\gamma_{h_1},\theta_1)g^*_{j_2}(\gamma_{h_2},\theta_2)\right\rangle_e$$
$$e^{i\left[x_1\gamma_{h_1}\cos(\theta_1)+y_1\gamma_{h_1}\sin(\theta_1)-\omega_{j_1}t\right]}e^{-i\left[x_2\gamma_{h_2}\cos(\theta_2)+y_2\gamma_{h_2}\sin(\theta_2)-\omega_{j_2}t\right]}\mathrm{d}\theta_1\mathrm{d}\theta_2\,\gamma_{h_1}\,\gamma_{h_2}\mathrm{d}\gamma_{h_1}\mathrm{d}\gamma_{h_2}. \quad (58)$$

The statistical properties of internal-wave modes are now exploited with respect to mode number, wavenumber, and propagation direction. First, internal waves arriving from different directions are generated by unrelated physical processes that are widely separated spatially. Therefore such arrivals are assumed to be statistically uncorrelated, $\left\langle g_{j_1}(\gamma_{h_1},\theta_1)g^*_{j_2}(\gamma_{h_2},\theta_2)\right\rangle_e = 0, \quad \theta_1 \neq \theta_2$. Second, second-order statistics of the generating mechanisms are assumed to be uniform in azimuth, $\left\langle \left|g_j(\gamma_h,\theta)\right|^2\right\rangle_e = G_j(\gamma_h),\ \forall\theta$. Third, because the internal-wave modes are uncoupled, the mode-amplitude fluctuations are statistically independent, $\left\langle g_{j_1}(\gamma_{h_1},\theta_1)g^*_{j_2}(\gamma_{h_2},\theta_2)\right\rangle_e = 0, \quad j_1 \neq j_2$. Fourth, linear internal-wave amplitude fluctuations are assumed to be governed by an orthogonal stationary stochastic process [39], $\left\langle g_j(\gamma_{h_1},\theta_1)g^*_j(\gamma_{h_2},\theta_2)\right\rangle_e = 0, \quad \gamma_{h_1} \neq \gamma_{h_2}$. With these statistical assumptions, the internal-wave power spectrum simplifies to

$$\left\langle g_{j_1}(\gamma_{h_1},\theta_1)g^*_{j_2}(\gamma_{h_2},\theta_2)\right\rangle_e = G_j(\gamma_h)\delta_{j_1j_2}\delta(\gamma_{h_1}-\gamma_{h_2})\frac{\delta(\theta_1-\theta_2)}{\gamma_h}, \quad (59)$$

and the correlation function of the horizontal wavenumbers becomes

$$\rho_m(\Delta_x,\Delta_y) = \left(\frac{\bar{k}^2}{\bar{\kappa}_m^2}\right)^2 \sum_{j=1}^{N}\int_0^\infty \mathscr{N}^2_{m,j}(\gamma_h)G_j(\gamma_h)\int_0^{2\pi} e^{i\gamma_h\Delta_x\cos(\theta)}e^{i\gamma_h\Delta_y\sin(\theta)}\mathrm{d}\theta\,\gamma_h\mathrm{d}\gamma_h. \quad (60)$$

4.4 Internal-Wave Spectrum

The relationship between acoustic and internal-wave spectra is finally obtained by substituting Eq. (60) into Eq. (50),

$$S_m(\gamma_h) = \frac{1}{2\pi|\gamma_h|}\left(\frac{\bar{k}^2}{\bar{\kappa}_m^2}\right)^2 \sum_{j=1}^{N}\int_0^\infty \mathscr{N}^2_{m,j}(\gamma_{h'})G_j(\gamma_{h'})\int_0^{2\pi}\int_{-\infty}^{\infty} e^{i\gamma_{h'}\Delta_x\cos(\theta)}\mathrm{d}\Delta_x$$
$$\int_{-\infty}^{\infty} e^{i\gamma_{h'}\Delta_y\sin(\theta)}e^{-i\gamma_h\Delta_y}\mathrm{d}\Delta_y\mathrm{d}\theta\,\gamma_{h'}\mathrm{d}\gamma_{h'}. \quad (61)$$

Note here that $\gamma_{h'} \geq 0$ because of the limits of integration. Thus $\gamma_{h'}$ may be replaced by $|\gamma_{h'}|$ within the integral. Then recognizing that

$$\int_{-\infty}^{\infty} e^{i\gamma_{h'}\Delta_x\cos(\theta)}\mathrm{d}\Delta_x = 2\pi\delta(\gamma_{h'}\cos(\theta)), \quad (62)$$

and that $\delta(\gamma_{h'}\cos(\theta))$ is nonzero for $\gamma_{h'} > 0$ only when $\theta = 2n\pi \pm \pi/2$, transverse wavenumbers are again selected; likewise:

$$\int_{-\infty}^{\infty} e^{\pm i\gamma_{h'}\Delta_y} e^{-i\gamma_h\Delta_y} \mathrm{d}\Delta_y = 2\pi\delta(\pm\gamma_{h'} - \gamma_h). \tag{63}$$

With these observations, the spectral relationship Eq. (61) becomes

$$S_m(\gamma_h) = \frac{2\pi}{|\gamma_h|}\left(\frac{\bar{k}^2}{\bar{\kappa}_m^2}\right)^2 \sum_{j=1}^{N} \int_0^{\infty} \mathscr{N}_{m,j}^2(\gamma_{h'}) G_j(\gamma_{h'}) \left[\delta(\gamma_{h'} - \gamma_h) + \delta(\gamma_{h'} + \gamma_h)\right] |\gamma_{h'}| \mathrm{d}\gamma_{h'}. \tag{64}$$

The properties of the delta functions imply $\gamma_h = \pm\gamma_{h'}$. But because $\gamma_{h'} \geq 0$, one delta function defines the positive half spectrum $S_m(\gamma_h \geq 0)$, and the other the negative half spectrum $S_m(\gamma_h \leq 0)$. Although the $S_m(\gamma_h = 0)$ component is counted twice, it is zero. Hence the spectrum simplifies to

$$S_m(\gamma_h) = 2\pi\left(\frac{\bar{k}^2}{\bar{\kappa}_m^2}\right)^2 \sum_{j=1}^{N} \mathscr{N}_{m,j}^2(\gamma_h) G_j(\gamma_h). \tag{65}$$

Then substituting Eq. (65) into Eq. (46), an expression for the modal phase-structure function is obtained in terms of the internal-wave spectra,

$$D_m(\Delta_y) = H_m \sum_{j=1}^{N} \int_0^{\infty} \mathscr{N}_{m,j}^2(\gamma_h) G_j(\gamma_h) \left[1 - \mathrm{sinc}(\gamma_h\Delta_y)\right] \gamma_h \mathrm{d}\gamma_h, \tag{66}$$

where $H_m \equiv 16\pi^2 x_o \bar{k}^4 / \bar{\kappa}_m^2$.

An observation of the coherence dependence on acoustic mode number may now be made. Because the horizontal acoustic wavenumbers $\bar{\kappa}_m$ decrease with increasing acoustic mode number m, the phase-structure function, Eq. (66), increases with mode number causing the exponential in the modal coherence function, Eq. (20), to fall off faster with transverse separation for the higher modes than for the lower modes. Likewise, H_m increases with total wavenumber $\bar{k}$ as the frequency rises, again causing a loss of coherence. It remains now to introduce an appropriate shallow-water model for the internal-wave spectrum $G_j(\gamma_h)$.

4.5 Internal-Wave Spectral Model

A definitive description of the internal-wave spectrum in shallow water remains an open question. Thus any choice is somewhat arbitrary. One candidate is a modification of the Garrett–Munk spectrum [50] for shallow water. While the mechanism for the generation of nonlinear internal waves by tidal flow across the continental shelf break is well established [22, 51, 52], the generation of diffuse shallow-water internal waves is less well understood. One source of such waves is the arrival from afar of diffuse deep-water linear internal waves that were generated in the open ocean. This latter process provides some justification for adapting the Garrett–Munk spectrum to shallow water as was done by Yang and Yoo [53]. However, it must be kept in mind that both the deep-water Garrett–Munk spectrum and especially any shallow-water modifications are based on empirical analyses.

Following the standard definition of the Garrett–Munk spectrum [41, 50], and using Eq. (53) with Eqs. (59) and (55) to obtain the variance of internal-wave displacements $\left\langle |\zeta|^2 \right\rangle$, the energy per unit area of ocean floor $\mathscr{E}$ $\left(\mathrm{J/m^2}\right)$ is given by

$$\mathscr{E} = \bar{\rho} \int_0^{z_o} N^2(z) \left\langle |\zeta(x,y;z,t)|^2 \right\rangle_e \mathrm{d}z \tag{67}$$

$$= 2\pi\bar{\rho} \sum_{j=1}^{N} \int_0^{\infty} G_j(\gamma_h)\, \gamma_h \mathrm{d}\gamma_h, \tag{68}$$

where $\bar{\rho}$ is a global mean density scale. In the same references, the Garrett–Munk spectrum $E_j(\gamma_h)$ is defined to satisfy

$$\mathscr{E} = \sum_{j=1}^{N} \int_0^{\infty} E_j(\gamma_h) \mathrm{d}\gamma_h. \tag{69}$$

(Note: The Garrett and Munk spectrum in Flatté et al. [25, p. 56] includes the density in their Eq. 3.2.22 for the internal-wave eigenfunction normalization, whereas here the standard normalization given by Eq. (55) does not.) Thus the relationship between the Garrett–Munk spectrum and the internal-wave spectrum as defined in this paper is

$$E_j(\gamma_h) = 2\pi\bar{\rho}\,\gamma_h G_j(\gamma_h). \tag{70}$$

The Garrett–Munk spectrum of each internal-wave mode has the form

$$E_j(\gamma_h) = E_0 \tilde{M}_j \tilde{E}_j(\gamma_h), \tag{71}$$

where E_0 is the total internal-wave energy density in shallow water, $E_0\tilde{M}_j$ is the energy of each mode, and

$$\tilde{M}_j \equiv M \left(j^2 + j_*^2\right)^{-p/2} \tag{72}$$

is the normalized partition of energy among modes with constant M defined such that $\sum_{j=1}^{N} \tilde{M}_j = 1$. Reasonable estimates of the constants are $j_* = 1$ and $p = 4$ for shallow-water internal waves [53]. For the deep-water Garrett–Munk spectrum [9], the constants are $j_* = 3$ and $p = 2$.

$\tilde{E}_j(\gamma_h)$ is either the normalized deep-water Garrett–Munk spectrum

$$\tilde{E}_j(\gamma_h) \equiv \frac{Q_j \gamma_j \gamma_h^2}{\left(\gamma_h^2 + \gamma_j^2\right)^2}, \tag{73}$$

or the Yang–Yoo version modified for shallow water [53],

$$\tilde{E}_j(\gamma_h) \equiv \frac{Q_j \gamma_j \gamma_h^2}{\left(\gamma_h^2 + \gamma_j^2\right)^{3/2} \left(\gamma_h^2 + (\gamma_j \bar{N}/f_c)^2\right)^{1/2}}. \tag{74}$$

The normalization constant Q_j is chosen such that $\int_0^\infty \tilde{E}_j(\gamma_h)\mathrm{d}\gamma_h = 1$. For the shallow-water form, f_c is the Coriolis frequency, the wavenumber spectrum peaks near $\gamma_j \equiv \pi j f_c/\bar{N}z_o$, and the average buoyancy frequency is defined as $\bar{N} \equiv z_o^{-1}\int_0^{z_o} N(z)\mathrm{d}z$.

Substitution of the Garrett–Munk internal-wave spectrum, Eqs. (70) and (71), into Eq. (65) produces a Garrett–Munk acoustic-mode fluctuation spectrum,

$$S_m(\gamma_h) = \frac{E_0}{\bar{\rho}\gamma_h}\left(\frac{\bar{k}^2}{\bar{\kappa}_m^2}\right)^2 \sum_{j=1}^{N} \tilde{M}_j \mathscr{N}_{m,j}^2(\gamma_h)\tilde{E}_j(\gamma_h). \tag{75}$$

Likewise, the phase-structure function, Eq. (66), in either deep or shallow water has the form

$$D_m(\Delta_y) = \frac{E_0 H_m}{2\pi\bar{\rho}} \sum_{j=1}^{N} \tilde{M}_j \mathscr{I}_{m,j}(\Delta_y), \quad \text{with} \tag{76}$$

$$\mathscr{I}_{m,j}(\Delta_y) \equiv \int_0^\infty \mathscr{N}_{m,j}^2(\gamma_h)\tilde{E}_j(\gamma_h)\,[1-\mathrm{sinc}(\gamma_h\Delta_y)]\,\mathrm{d}\gamma_h. \tag{77}$$

Immediately apparent is the direct dependence of the phase-structure function on E_0, which causes an associated loss of transverse coherence in the presence of energetic internal waves. The dependencies on $\tilde{M}_j$ and $\mathscr{N}_{m,j}$ imply the impact on acoustic coherence is most severe for the lowest internal-wave mode. It is the integral $\mathscr{I}_{m,j}(\Delta_y)$ that determines the *shape* of the phase structure as a function of Δ_y through the behavior of $[1-\mathrm{sinc}(\gamma_h\Delta_y)]$ as weighted by the spectral properties of the internal waves and buoyancy.

5. SIMULATED COHERENCE

To illustrate the behavior of the path-integral solution for the phase-structure function and the associated acoustic-field coherence that was developed in Ch. 3, it is necessary to obtain a somewhat realistic power spectrum for the eigenvalue fluctuations. The required spectrum is obtained by finding parameters for the Garrett–Munk spectrum of Sec. 4.5 that produce a reasonable fit to measured shallow-water internal-wave spectra.

5.1 Experimental Spectra

For the above purposes, three spectra were used that were obtained by experiments in the Barents Sea (Barents) [54, 55], the Mid-Atlantic Bight (SWARM) [23], and the East China Sea (TAVEX) [56, 57]. These environments provided a diverse set of spectra, with Barents emphasizing low wavenumbers, SWARM mid wavenumbers, and TAVEX high wavenumbers.

5.1.1 SWARM and Barents Spectra

Some preliminary comments concerning the SWARM spectra are necessary. The SWARM spectra were estimated from vertical-velocity fluctuations obtained from a bottom-mounted acoustic Doppler current profiler (ADCP). An empirical orthogonal function (EOF) decomposition of the fluctuations was done, and the frequency-domain spectrum of the lowest empirical mode was presented in Fig. 19 of Ref. 23. Due to an

error in that figure, the published power spectral density is too large by a factor of 480 [58]. Corrections for this error were made before any further processing of the SWARM spectrum.

The spectra published for Barents [54, Fig. 9] and SWARM [23, Fig. 19] are both plotted as displacement variance $\left(\mathrm{m}^2/\mathrm{cpd}\right)$ versus frequency in cycles-per-day (cpd). These figures were digitized by hand and converted to units of energy density per wavenumber. First the spectra were rescaled by a factor of $86400/2\pi$ to convert the units to $\mathrm{m}^2/\left(\mathrm{rad}/\mathrm{s}\right)$.

Next, the spectra were converted from the frequency to the wavenumber domain under the assumption that these environments are dominated by the first internal-wave mode, i.e., $j = 1$ in what follows. Let $S_j(\omega)$ with units $\mathrm{m}^2/\left(\mathrm{rad}/\mathrm{s}\right)$ represent the frequency-domain displacement spectra. Then because $S_j(\omega)\mathrm{d}\omega = S_j(\gamma_h)\mathrm{d}\gamma_h$, the wavenumber domain spectrum is $S_j(\gamma_h) = S_j(\omega)v_g^j(\gamma_h)$, where $v_g^j(\gamma_h) = \partial\omega_j(\gamma_h)/\partial\gamma_h$ is the modal group speed; $S_j(\gamma_h)$ now has units $\mathrm{m}^2/\left(\mathrm{rad}/\mathrm{m}\right)$. The required group speeds were obtained by solving the internal-wave Sturm–Liouville problem [25, 44, 59] using the density profiles reported for the experiments' environments.

Finally, the displacement spectra were converted to energy spectra by recognizing that $S_j(\gamma_h)$ is the spectrum of a variance, which can be substituted into a wavenumber-domain transform of Eq. (67),

$$F_j(\gamma_h) = \bar{\rho}S_j(\gamma_h)\int_0^{z_o} N^2(z)\mathrm{d}z, \tag{78}$$

where $F_j(\gamma_h)$ is an energy spectrum with the same units $\left(\mathrm{J}/\mathrm{m}^2\right)/\left(\mathrm{rad}/\mathrm{m}\right)$ as the Garrett–Munk spectrum. With the above relationships, the frequency-domain power spectral density presented in the Barents and SWARM papers were digitized and converted to a wavenumber-domain energy spectrum for comparison with the Garrett–Munk spectrum.

5.1.2 TAVEX Spectra

The Transverse Acoustic Variability Experiment (TAVEX) [60] took place in the East China Sea during August 2008. The objective of the experiment was to obtain data concerning the impact of dynamic ocean processes on the coherence of acoustic fields along a direction transverse to the main path of acoustic propagation. In support of that, a vertical conductivity, temperature, and depth (CTD) chain with sensors at fixed intervals of depth was towed along a series of straight-line tracks. Because the track data were analyzed in 3 km segments, obtaining reliable estimates of low-wavenumber components of the spectra are precluded in this environment. However, these sensors were able to provide measurements of high-wavenumber fluctuations as a function of horizontal position. From the density fluctuations the variance of vertical displacement, and the spectrum of that, were obtained as follows. The relationship between density fluctuations and small vertical displacements due to linear internal waves is

$$\delta\rho(y,z) = \frac{\partial_p\bar{\rho}(z)}{\partial z}\zeta(y,z), \tag{79}$$

where $\delta\rho(y,z) = \rho(y,z) - \bar{\rho}(z)$ is the density perturbation, $\zeta(y,z)$ is the internal-wave displacement, and $\partial_p\bar{\rho}(z)/\partial z$ is the *potential* gradient of the mean density profile $\bar{\rho}(z) = \langle\rho(y,z)\rangle_y$. Note that with these

definitions both $\delta\rho(y,z)$ and $\zeta(y,z)$ are zero mean. In shallow water where pressure corrections are small, a reasonable approximation of buoyancy frequency squared [44, 59] is

$$\bar{N}^2(z) \equiv \frac{g}{\bar{\rho}(z)} \frac{\partial_p \bar{\rho}(z)}{\partial z}. \tag{80}$$

Equation (79) was solved for $\zeta(y,z)$ and Fourier transformed over the transverse dimension, y, to obtain the power spectral density $S(\gamma_h,z)$ of the displacement variance as a function of horizontal wavenumber and depth. As was done for the SWARM data for Eq. (78), this was substituted into Eq. (67), but this time taking depth variability into account:

$$F(\gamma_h) = \int_0^{z_o} \bar{\rho}(z) N^2(z) S(\gamma_h,z) \mathrm{d}z. \tag{81}$$

5.1.3 Spectra Discussion

Internal-wave energy spectra, estimated using the above procedures, are shown in Fig. 2. Here in the log–log wavenumber domain, the spectra lie along a common power-law line with a slope that is approximately -2. The bump in the SWARM spectrum between wavenumbers 10^{-2} and 10^{-1} rad/m was attributed to nonlinear internal waves by Apel et al. [23]. The rise in the TAVEX spectrum at the highest wavenumbers is likely aliasing due to contamination by fine-scale features such as spice, which were observed by the CTD chain [61].

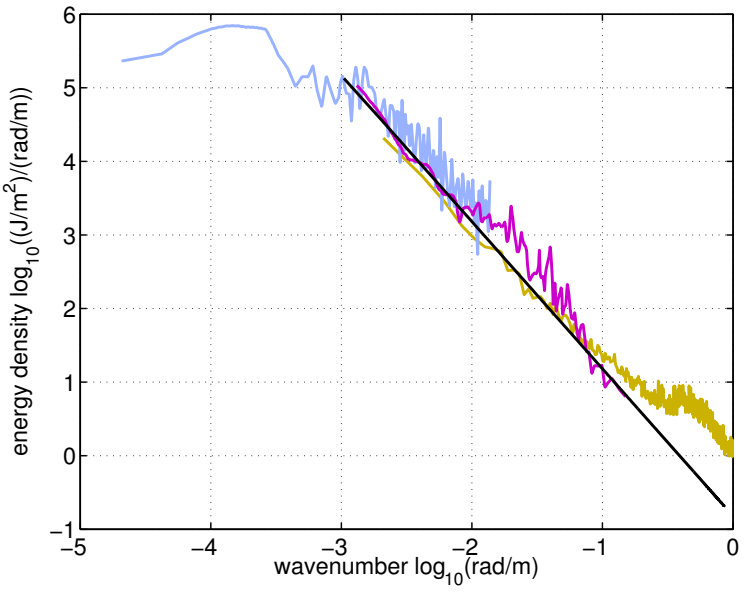

Fig. 2 — Empirical best-fit Garrett–Munk spectrum (black) with $E0 = 200$ J/m^2, deep-water $\tilde{E}_j(\gamma_h)$, and shallow-water $j_* = 1$ with $p = 4$. For comparison, spectra are shown for TAVEX (brown), SWARM (magenta), and Barents (blue).

A Garrett–Munk spectrum was empirically fit to the experimental data. The parameters that best describe the spectrum include a large energy density of $E0 = 200\ \mathrm{J/m^2}$, which is seemingly more appropriate for shelf-break regions with water depths on the order of 200 m, than shallow shelf areas where the energy is expected to be an order of magnitude less. The spectral slope is also odd, being best fit with the deep-water spectrum for $\tilde{E}_j(\gamma_h)$ given by Eq. (73). The choice of shallow-water coefficients, $j_* = 1$ and $p = 4$, merely emphasizes the first mode above all others.

It must be noted here that both the SWARM and TAVEX experiments, though situated upslope, were in the vicinity of shelf breaks at 200 m depth where internal waves are known to be generated [52, 62, 63], and the water depth across the Barents site spanned 100–400 m. So the parameters, although unusual, are not entirely unjustifiable. And while the parameters of this fit may be debatable on physical grounds, the resulting spectrum does mimic the data closely enough to provide a reasonable simulation of the acoustic-mode fluctuation spectrum, Eq. (75), that is required by the phase-structure function, Eqs. (76) and (77).

5.2 Coherence Discussion

Prior to discussion, a few words need to be said about acoustic and internal-wave mode functions. To determine the acoustic coherence function it is necessary to evaluate the modal interaction described by Eq. (57), which requires suitable acoustic and internal-wave modes. Because the TAVEX environment was recently measured by the author, it was chosen to provide those modes. Acoustic modes were computed by the Kraken program of Porter [64], and internal-wave modes were computed using a program by Bell, Jr. [65].

Computation of the acoustic coherence function also requires the partition of acoustic energy among modes as prescribed by Eq. (21). The necessary mode amplitudes were obtained by projecting a complex acoustic field from the RAM parabolic equation model of Collins [66–68] onto the acoustic mode functions from Kraken. Figure 3 shows the partition of intensities among modes at 500 Hz. Clearly the lowest acoustic modes have the most weight, so their properties tend to dominate the combined acoustic coherence.

In comments following Eq. (66), it was pointed out that the phase-structure function increases with mode number. This behavior is seen in Fig. 4 where the amplitude of the phase-structure function increases much more rapidly for mode 7 (black) than for mode 1 (blue), which remains flat-lined. Also apparent in this figure is the approach to saturation at a range of 5 km with decaying undulations caused by the sinc function in Eq. (46). Obviously, the modal coherence functions must mirror this behavior (Fig. 5) because they are the negative exponentials of the phase-structure functions, cf. Eq. (20).

The total acoustic coherence shown in Fig. 6 is the weighted sum, Eq. (21), of the modal coherences. In this figure it is seen that the coherence falls off more rapidly with transverse separation at 500 Hz than at 300 Hz. This observation is in line with the comments following Eq. (66), where such behavior was predicted. In comparing the 500 Hz total coherence (blue) to the modal coherences in Fig. 5 it is seen that the total coherence, as the weighted sum of all modes, behaves in this case much like mode 4 (cyan).

The power-law behavior of the coherence, n, discussed at the end of Sec. 2.1, can be obtained by twice taking the logarithm of Eq. (9) and substituting Eq. (10),

$$\Lambda_P(y) \equiv \ln\left(-2\ln\left(\tilde{R}_P(\Delta y)\right)\right) = \ln D_P(\Delta y), \tag{82}$$

$$= n\ln\Delta y - n\ln L. \tag{83}$$

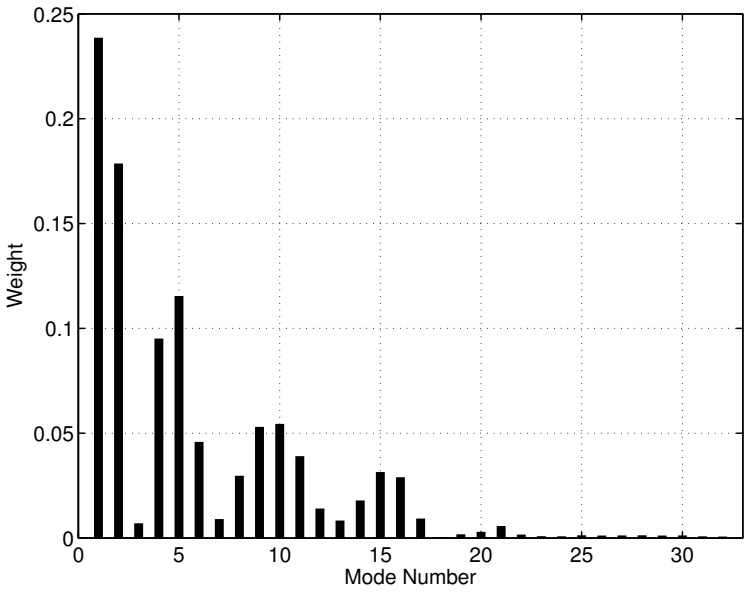

Fig. 3 — Partition of acoustic intensity among modes for 500 Hz signals

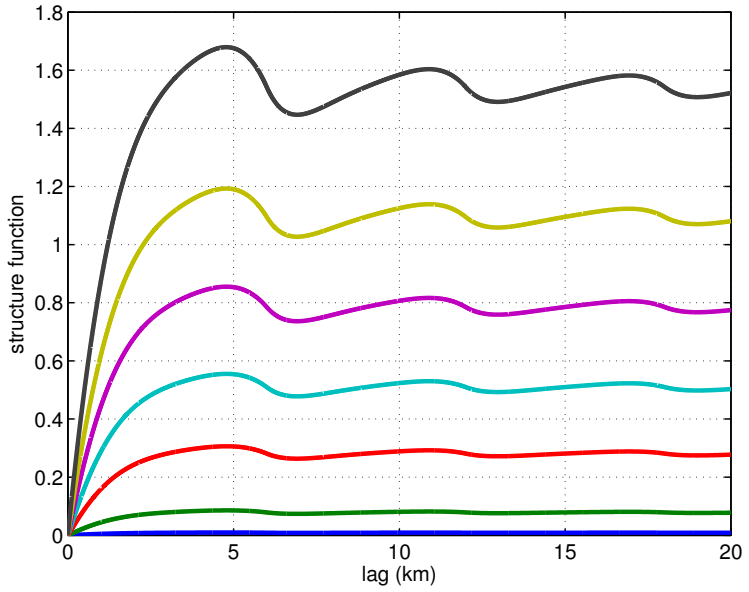

Fig. 4 — Modal phase-structure functions for 500 Hz acoustic modes 1–7 colored in order blue to black

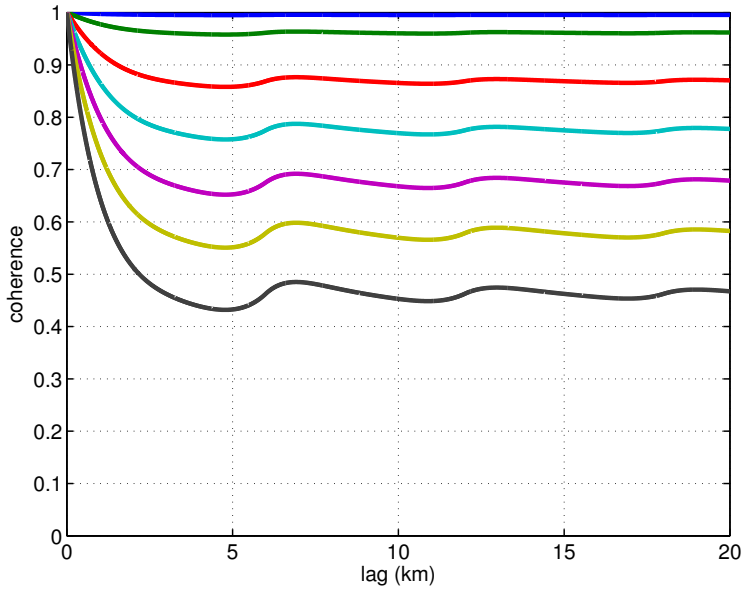

Fig. 5 — Modal coherence functions for 500 Hz acoustic modes 1–7 colored in order blue to black

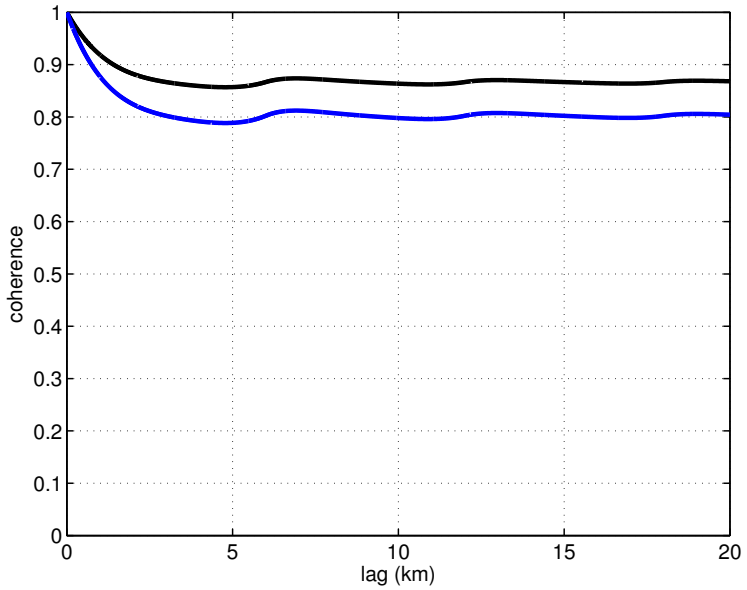

Fig. 6 — Phone coherence at 300 Hz (black) and 500 Hz (blue)

The resulting theoretical power-law behavior, shown in Fig. 7, has a slope of $n = -2$ for small separations, as expected from the properties of the sinc function in Eq. (46). But this slope flattens out as the coherence saturates to the scattering intensity at large separations. The simple power law described by Eq. (10) only holds for small separations.

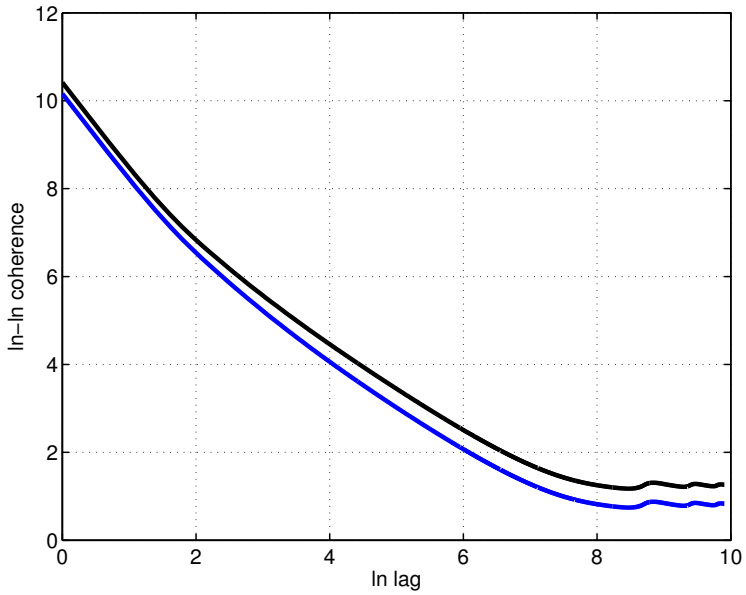

Fig. 7 — Log–log coherence power law $\Lambda_P(\ln(y))$ from Eq. (83) shown for 300 Hz (black) and 500 Hz (blue)

The coherence presented in these numerical evaluations of path-integral theory decays much more slowly than is found in experimental measurements. These results are clearly at odds with a significant body of the literature. Carey [29] reported a comprehensive list of coherence lengths in various seas in the 135–600 Hz band, with deep-water lengths on the order of 100λ over 500 km, and shallow-water coherence about 30λ over 45 km. In the Levantine Sea, Carey [69] found coherence lengths on the order of 543, 231, and 116 m at frequencies of 58, 175, and 348 Hz, respectively. For observations of transverse coherence at a range of 40 km in the Strait of Korea, Carey et al. [30] found coherence lengths of 112 m at 400 Hz. For deep-water data obtained in the Pacific, Andrew et al. [15] observed coherence lengths on the order of 410–528 m at ranges between 2000 and 3000 km. These results were obtained assuming a power-law phase-structure function like Eq. (10) with $n = 3/2$ that was based on the work of Flatté and Stoughton [26].

6. SUMMARY

The mutual-coherence function was found in Eq. (8) to be described by a normalized amplitude correlation function multiplied by the phase-structure function. In shallow water where the acoustic field is naturally described by a linear combination of normal modes, the mutual-coherence function was shown to be a sum of modal coherence functions, each of which is governed by a modal phase-structure function.

Formulation of the transverse coherence problem using mode amplitudes propagating in the horizontal plane is advantageous because the ray paths are nearly straight lines with no interaction with lateral boundaries. These conditions justify using the parabolic and Markov approximations required by the path-integral approach. Conversely, the modal approach breaks down near caustics that form in the vicinity where modes become evanescent.

For isotropic internal-wave fields, fluctuations with wavevectors parallel to the acoustic path were found in Sec. 3.3 to produce a delta function, $\delta(\gamma_h \cos(\theta))$, that selects only the $\theta = \pm\pi/2$ components of the internal-wave spectrum, thus showing that the transverse acoustic coherence depends solely on the transverse part of the internal-wave spectrum.

The impact of internal waves on acoustic modes is proportional to the internal-wave energy $E0$, and was found in Eq. (57) to depend on how the shape of the acoustic mode function aligns with the internal-wave excitation. This interaction is strongest for the lowest internal-wave modes, which have maxima in regions of high buoyancy, and is weakest for high-order internal-wave modes that oscillate rapidly at the same depth. Likewise, acoustic modes with maxima in the vicinity of high buoyancy suffer more severe coherence loss than modes with a null near the gradient. The highest acoustic modes are also subject to rapid loss of coherence because of the inverse dependence of the phase-structure function on the horizontal acoustic wavenumbers, as shown in Eq. (66).

Although the theory presented herein is perhaps less than fully satisfying because of the simplifications required to make progress (adiabatic modes, homogeneous isotropic internal-wave spectra, the Markov approximation, and the Garrett–Munk spectrum), it is nevertheless a complete theory that quantitatively relates the transverse acoustic coherence function to the underlying internal-wave field. As such, it provides predictive capabilities that illuminate several aspects of the relationship. Chief among these is the result expressed by Eq. (46) that the transverse acoustic coherence is determined by transverse fluctuations in the underlying sound-speed field, as expressed by an integral over the fluctuation spectrum *weighted by a sinc function*. It is the sinc function that provides the correct transition between the phase-structure function at small hydrophone separations and the scattering strength at large separations.

Results show the coherence predicted by path-integral theory as applied to the transverse scattering of normal modes appears to decay too slowly with hydrophone separation to describe the observed ocean. In contradistinction to experimental measurements, saturation effects described by the theory only become significant at very large separations spanning several kilometers.

ACKNOWLEDGMENTS

This work was supported by the Office of Naval Research (ONR). The author sincerely thanks T. C. Yang, Steven Finette, and Altan Turgut for their constructive comments.

REFERENCES

1. D. C. Whitmarsh, E. Skudrzyk, and R. J. Urick, "Forward scattering of sound in the sea and its correlation with the temperature microstructure," *J. Acoust. Soc. Am.* **29**(10), 1124–1142 (1957).

2. E. Skudrzyk, "Scattering in an inhomogeneous medium," *J. Acoust. Soc. Am.* **29**(1), 50–58 (1957).

3. O. S. Lee, "Effect of an internal wave on sound in the ocean," *J. Acoust. Soc. Am.* **33**(5), 677–681 (1961).

4. O. S. Lee, "Observations on internal waves in shallow water," *Limnology and Oceanography* **6**(3), 312–321 (1961).

5. C. W. Ufford, "Internal waves measured at three stations," rept., Division of War Research at the U.S. Navy Radio and Sound Laboratory, University of California (1945).

6. C. W. Ufford, "Internal waves measured at three stations," *Trans. Am. Geophys. Union* **28**, 87–95 (1947).

7. H. A. DeFerrari, "Effects of horizontally varying internal wavefields on multipath interference for propagation through the deep sound channel," *J. Acoust. Soc. Am.* **56**(1), 40–46 (1974).

8. S. M. Flatté and F. D. Tappert, "Calculation of the effect of internal waves on oceanic sound transmission," *J. Acoust. Soc. Am.* **58**(6), 1151–1159 (1975).

9. W. H. Munk and F. Zachariasen, "Sound propagation through a fluctuating stratified ocean: Theory and observation," *J. Acoust. Soc. Am.* **59**(4), 818–838 (1976).

10. S. M. Flatté, "Wave propagation through random media: Contributions from ocean acoustics," *Proc. IEEE* **71**(11), 1267–1294 (1983).

11. R. Dashen, "Path integrals for waves in random media," *J. Math. Phys.* **20**(5), 894–920 (1979).

12. R. Esswein and S. M. Flatté, "Calculation of the phase-structure function density from oceanic internal waves," *J. Acoust. Soc. Am.* **70**(5), 1387–1396 (1981).

13. J. A. Colosi, "A review of recent results on ocean acoustic wave propagation in random media: Basin scales," *IEEE J. Ocean. Eng.* **24**(2), 138–155 (1999).

14. S. M. Flatté and G. Rovner, "Calculations of internal-wave-induced fluctuations in ocean-acoustic propagation," *J. Acoust. Soc. Am.* **108**(2), 526–534 (2000).

15. R. K. Andrew, B. M. Howe, and J. A. Mercer, "Transverse horizontal spatial coherence of deep arrivals at megameter ranges," *J. Acoust. Soc. Am.* **117**(3), 1511–1526 (2005).

16. J. A. Colosi, A. B. Baggeroer, B. D. Cornuelle, M. A. Dzieciuch, W. H. Munk, P. F. Worcester, B. D. Dushaw, B. M. Howe, J. A. Mercer, R. C. Spindel, T. G. Birdsall, K. Metzger, and A. M. G. Forbes, "Analysis of multipath acoustic field variability and coherence in the finale of broadband basin-scale transmissions in the North Pacific Ocean," *J. Acoust. Soc. Am.* **117**(3), 1538–1564 (2005).

17. J. A. Colosi and S. M. Flatté, "Mode coupling by internal waves for multimegameter acoustic propagation in the ocean," *J. Acoust. Soc. Am.* **100**(6), 3607–3620 (1996).

18. A. G. Voronovich and V. E. Ostashev, "Coherence function of a sound field in an oceanic waveguide with horizontally isotropic statistics," *J. Acoust. Soc. Am.* **125**(1), 99–110 (2009).

19. J. C. Preisig and T. F. Duda, "Coupled acoustic mode propagation through continental-shelf internal solitary waves," *IEEE J. Ocean. Eng.* **22**(2), 256–269 (1997).

20. T. F. Duda and J. C. Preisig, "A modeling study of acoustic propagation through moving shallow-water solitary wave packets," *IEEE J. Ocean. Eng.* **24**(1), 16–32 (1999).

21. T. F. Duda, "Temporal and cross-range coherence of sound traveling through shallow-water nonlinear internal wave packets," *J. Acoust. Soc. Am.* **119**(6), 3717–3725 (2006).

22. S. Finette, M. H. Orr, A. Turgut, J. R. Apel, M. Badiey, C.-S. Chiu, R. H. Headrick, J. N. Kemp, J. F. Lynch, A. E. Newhall, B. Pasewark, S. N. Wolf, and D. Tielbürger, "Acoustic field variability induced by time evolving internal wave fields," *J. Acoust. Soc. Am.* **108**(3), 957–972 (2000).

23. J. R. Apel, M. Badiey, C.-S. Chiu, S. Finette, R. Headrick, J. Kemp, J. F. Lynch, A. Newhall, M. H. Orr, B. H. Pasewark, D. Tielbürger, A. Turgut, K. von der Heydt, and S. Wolf, "An overview of the 1995 SWARM shallow-water internal wave acoustic scattering experiment," *IEEE J. Ocean. Eng.* **22**(3), 465–500 (1997).

24. S. Finette and R. Oba, "Horizontal array beamforming in an azimuthally anisotropic internal wave field," *J. Acoust. Soc. Am.* **114**(1), 131–144 (2003).

25. S. M. Flatté, R. Dashen, W. H. Munk, K. M. Watson, and F. Zachariasen, *Sound Transmission Through A Fluctuating Ocean* (Cambridge University Press, Cambridge, England, 1979).

26. S. M. Flatté and R. B. Stoughton, "Predictions of internal-wave effects on ocean acoustic coherence, travel-time variance, and intensity moments for very long-range propagation," *J. Acoust. Soc. Am.* **84**(4), 1414–1424 (1988).

27. R. Dashen, S. M. Flatté, and S. A. Reynolds, "Path-integral treatment of acoustic mutual coherence functions for rays in a sound channel," *J. Acoust. Soc. Am.* **77**(5), 1716–1722 (1985).

28. H. Cox, "Line array performance when the signal coherence is spatially dependent," *J. Acoust. Soc. Am.* **54**(6), 1743–1746 (1973).

29. W. M. Carey, "The determination of signal coherence length based on signal coherence and gain measurements in deep and shallow water," *J. Acoust. Soc. Am.* **104**(2), 831–837 (1998).

30. W. M. Carey, P. G. Cable, W. L. Siegmann, J. F. Lynch, and I. Rozenfeld, "Measurement of sound transmission and signal gain in the complex Strait of Korea," *IEEE J. Ocean. Eng.* **27**(4), 841–852 (2002).

31. F. B. Jensen, W. A. Kuperman, M. B. Porter, and H. Schmidt, *Computational Ocean Acoustics* (American Institute of Physics Press, Woodbury, NY, 1994).

32. A. D. Pierce, "Extension of the method of normal modes to sound propagation in an almost-stratified medium," *J. Acoust. Soc. Am.* **37**(1), 19–27 (1965).

33. H. Weinberg and R. Burridge, "Horizontal ray theory for ocean acoustics," *J. Acoust. Soc. Am.* **55**(1), 63–79 (1974).

34. R. Burridge and H. Weinberg, "Horizontal rays and vertical modes," in J. B. Keller and J. S. Papadakis, eds., *Wave Propagation and Underwater Acoustics*, pp. 86–152 (Springer-Verlag, Berlin, 1977).

35. Y. S. Shifrin, *Statistical Antenna Theory* (Golem Press, Boulder, CO, 1971).

36. V. I. Tatarskii, *The Effects of the Turbulent Atmosphere on Wave Propagation* (U.S. Department of Commerce, NTIS, Springfield, VA, 1971).

37. P. C. Mignerey, "Environmentally adaptive wedge modes," *J. Acoust. Soc. Am.* **107**(4), 1944–1952 (2000).

38. E. K. Westwood, "Ray model solutions to the benchmark wedge problems," *J. Acoust. Soc. Am.* **87**(4), 1539–1545 (1990).

39. M. B. Priestley, *Spectral Analysis and Time Series* (Academic Press, London, UK, 1981).

40. B. G. Katsnelson and V. G. Petnikov, *Shallow-Water Acoustics* (Springer-Praxis, Chichester, UK, 2002).

41. J. A. Colosi and M. G. Brown, "Efficient numerical simulation of stochastic internal-wave-induced sound-speed perturbation fields," *J. Acoust. Soc. Am.* **103**(4), 2232–2235 (1998).

42. P. F. Worcester, G. O. Williams, and S. M. Flatté, "Fluctuations of resolved acoustic multipaths at short range in the ocean," *J. Acoust. Soc. Am.* **70**(3), 826–840 (1981).

43. S. A. Reynolds, S. M. Flatté, R. Dashen, B. Buehler, and P. Maciejewski, "Afar measurements of acoustic mutual coherence functions of time and frequency," *J. Acoust. Soc. Am.* **77**(5), 1723–1731 (1985).

44. A. E. Gill, *Atmosphere–Ocean Dynamics* (Academic Press, New York, NY, 1982).

45. D. Tielbürger, S. Finette, and S. N. Wolf, "Acoustic propagation through an internal wave field in a shallow water waveguide," *J. Acoust. Soc. Am.* **101**(2), 789–808 (1997).

46. C. Garrett and W. Munk, "Space-time scales of internal waves," *Geophysical Fluid Dynamics* **2**, 225–264 (1972).

47. L. B. Dozier and F. D. Tappert, "Statistics of normal mode amplitudes in a random ocean: I. Theory," *J. Acoust. Soc. Am.* **63**(2), 353–365 (1978).

48. O. M. Phillips, *The Dynamics of the Upper Ocean* (Cambridge University Press, Cambridge, UK, 1977).

49. C. Eckart, *Hydrodynamics of Oceans and Atmospheres* (Pergamon Press, New York, NY, 1960).

50. C. Garrett and W. Munk, "Space-time scales of internal waves — progress report," *J. Geophys. Res.* **80**(3), 291–297 (1975).

51. M. H. Orr and P. C. Mignerey, "Nonlinear internal waves in the South China Sea: Observation of the conversion of depression internal waves to elevation internal waves," *J. Geophys. Res.* **108**(C3), 3064–3079 (2003).

52. S. Finette, R. Oba, C. Shen, and T. Evans, "Acoustic propagation under tidally driven, stratified flow," *J. Acoust. Soc. Am.* **121**(5), 2575–2590 (2007).

53. T. C. Yang and K. Yoo, "Internal wave spectrum in shallow water: Measurement and comparison with the Garrett–Munk model," *IEEE J. Ocean. Eng.* **24**(3), 333–345 (1999).

54. J. F. Lynch, G. Jin, R. Pawlowicz, D. Ray, A. J. Plueddenmann, C.-S. Chiu, J. H. Miller, R. H. Bourke, A. R. Parsons, and R. Muench, "Acoustic travel-time perturbations due to shallow-water internal waves and internal tides in the Barents Sea polar front: Theory and experiment," *J. Acoust. Soc. Am.* **99**(2), 803–821 (1996).

55. A. R. Parsons, R. H. Bourke, R. D. Muench, C.-S. Chiu, J. F. Lynch, J. H. Miller, A. J. Plueddenmann, and R. Pawlowicz, "The Barents Sea polar front in summer," *J. Geophys. Res.* **101**(C6), 14201–14221 (1996).

56. P. C. Mignerey, "Application of path-integral theory to shallow-water coherence," in 24^{th} *Underwater Acoustics Conference, Acoust. Soc. Korea*, Jinhae, Korea, Sept. 2009 (Agency for Defense Development).

57. P. C. Mignerey and D. J. Goldstein, "Analysis of horizontal coherence during TAVEX," in 24^{th} *Underwater Acoustics Conference, Acoust. Soc. Korea*, Jinhae, Korea, Sept. 2009 (Agency for Defense Development).

58. C.-S. Chiu, Naval Postgraduate School, private communication, 2011.

59. J. R. Apel, *Principles of Ocean Physics* (Academic Press, San Diego, CA, 1987).

60. The Transverse Acoustic Variability Experiment (TAVEX) was a collaboration in the East China Sea during August 2008 that comprised: the U. S. Office of Naval Research (ONR), the U. S. Naval Research Laboratory (NRL), the R. O. K. Agency for Defense Development (ADD), the R. O. K. Naval Systems Research and Development Institute (NSRDI), the Korea Ocean Research and Development Institute (KORDI), the Applied Research Laboratory at The Pennsylvania State University (ARL-PSU), the Applied Physics Laboratory at the University of Washington (APL-UW), and Hanyang University (HU).

61. C. M. Smith, M. M. Kingsland, and D. L. Bradley, "Towed CTD chain data collection and acoustic propagaton predictions for the East China Sea," in 24^{th} *Underwater Acoustics Conference, Acoust. Soc. Korea*, Jinhae, Korea, Sept. 2009 (Agency for Defense Development).

62. K. G. Lamb, "Numerical experiments of internal wave generation by strong tidal flow across a finite amplitude bank edge," *J. Geophys. Res. (Oceans)* **99**(C1), 843–864 (1994).

63. C. Y. Shen and T. E. Evans, "A free-surface hydrodynamic model for density-stratified flow in the weakly to strongly non-hydrostatic regime," *J. Comput. Phys.* **200**, 695–717 (2004).

64. M. B. Porter, "The KRAKEN Normal Mode Program," SACLANTCEN Memorandum SM-245, SACLANT Undersea Research Centre, La Spezia, Italy (1991).

65. T. H. Bell, Jr., "Numerical Calculation of Dispersion Relations for Internal Gravity Waves," NRL Report 7294, Naval Research Laboratory, Washington, DC (1971).

66. M. D. Collins, "Generalization of the split-step Padé solution," *J. Acoust. Soc. Am.* **96**(1), 382–385 (1994).

67. M. D. Collins, R. J. Cederberg, D. B. King, and S. A. Chin-Bing, "Comparison of algorithms for solving parabolic wave equations," *J. Acoust. Soc. Am.* **100**(1), 178–182 (1996).

68. M. Porter, K. Smith, P. Baxley, S. Ivansson, I. Karasalo, and P. Gerstoft, "Ocean Acoustics Library," rept., U.S. Office of Naval Research, Arlington, VA (2010), URL http://oalib.hlsresearch.com/.

69. W. M. Carey, "Sonar array characterization, experimental results," *IEEE J. Ocean. Eng.* **23**(3), 297–306 (1998).

Appendix A

EIGENVALUE PERTURBATION EXPANSION

Following Rajan et al. [A1], a perturbation technique introduced by Schrödinger [A2] and discussed in several standard references [A3, A4] is used to relate stochastic fluctuations in the eigenvalues of the Helmholtz equation to those of the underlying index of refraction. First, perturbation expansions for the eigenvalues κ_m are introduced using Eq. (25), which has deterministic part $\bar{\kappa}_m(1+u_m(x,y))$ and small stochastic part $\bar{\kappa}_m\mu_m(x,y)$. Likewise, the total wavenumber k is expanded by letting

$$k(x,y;z) = \bar{k}\,(1+v(x,y;z)+\nu(x,y;z))\,. \tag{A1}$$

Here $1+v(z)\sim\mathscr{O}(1)$ is the deterministic wavenumber profile and $\nu(z)$ is a small stochastic fluctuation such that $\nu(z)\sim\mathscr{O}(\mu_m)\ll 1$. The eigenfunctions are represented as

$$\Psi_m(x,y;z) = \bar{\Psi}_m(z)+\mu_m\psi_m(x,y;z), \tag{A2}$$

where $\bar{\Psi}_m(z)$ are the deterministic eigenfunctions, and the $\mu_m\psi_m(x,y;z)$ are small stochastic functions.

A solution for the eigenvalue perturbations is obtained by rewriting Eq. (14) in operator form as

$$[H(z)-W_m]\,\Psi_m(z) = 0, \quad \text{where} \tag{A3}$$

$$H(z) \equiv \bar{\rho}(z)\frac{\partial}{\partial z}\left(\frac{1}{\bar{\rho}(z)}\frac{\partial}{\partial z}\right)+k^2(z), \quad \text{and} \tag{A4}$$

$$W_m = k_m^2. \tag{A5}$$

Using the above perturbation expansions and dropping quadratic products, the problem can be split into a large deterministic part (0) and a small stochastic part (1):

$$H(z) = H^{(0)}(z)+H^{(1)}(z), \tag{A6}$$

$$W_m = W_m^{(0)}+W_m^{(1)}, \tag{A7}$$

$$\Psi_m(z) = \Psi_m^{(0)}(z)+\Psi_m^{(1)}(z); \tag{A8}$$

where the various parts are defined as:

$$H^{(0)}(z) = \bar{\rho}(z)\frac{\partial}{\partial z}\left(\frac{1}{\bar{\rho}(z)}\frac{\partial}{\partial z}\right) + \bar{k}^2(1+2v(z)), \tag{A9}$$

$$H^{(1)}(z) = 2\bar{k}^2 v(z), \tag{A10}$$

$$W_m^{(0)} = \bar{\kappa}_m^2(1+2u_m), \tag{A11}$$

$$W_m^{(1)} = 2\bar{\kappa}_m^2\mu_m, \tag{A12}$$

$$\Psi_m^{(0)}(z) = \bar{\Psi}_m(z), \tag{A13}$$

$$\Psi_m^{(1)}(z) = \mu_m\psi_m(z). \tag{A14}$$

Following established procedures [A3, A4], first-order terms are collected and found to satisfy

$$\int_0^{z_o}\left[H^{(1)}(z) - W_m^{(1)}\right]{\Psi_m^{(0)}}^2(z)/\bar{\rho}(z)\mathrm{d}z = 0. \tag{A15}$$

REFERENCES

A1. S. D. Rajan, J. F. Lynch, and G. V. Frisk, "Perturbative inversion methods for obtaining bottom geoparameters in shallow water," *J. Acoust. Soc. Am.* **82**(3), 998–1017 (1987).

A2. E. Schrödinger, "Quantisierung als eigenwertproblem," *Ann. Physik* **80**(13), 437–490 (1926).

A3. L. I. Schiff, *Quantum Mechanics* (McGraw-Hill, New York, NY, 1968).

A4. F. B. Jensen, W. A. Kuperman, M. B. Porter, and H. Schmidt, *Computational Ocean Acoustics* (American Institute of Physics Press, Woodbury, NY, 1994).

Appendix B

LIST OF SYMBOLS

$<>_t$	ensemble average over time
$<>_y$	ensemble average over space
$<>_e$	ensemble average over environments
x	range from source
θ	transverse polar coordinate
$y = r\theta$	transverse Cartesian coordinate
z	depth below ocean surface
x_o	receiver range
z_o	receiver depth
Δy	transverse hydrophone separation
$\omega = 2\pi f$	acoustic frequency
$\mathbf{u} = (r, \theta, z)$	generalized coordinate vector
$c(\mathbf{u})$	sound speed
$\bar{c}$	mean sound-speed scale
$k(\mathbf{u})$	acoustic wavenumber
$P(\mathbf{u})$	complex acoustic pressure
$\tilde{P}(y)$	complex acoustic phase
σ_P^2	acoustic pressure intensity
$\sigma_{A_m}^2$	acoustic mode intensity
L	empirical coherence length
n	empirical coherence power-law
Φ	scattering strength
$\delta\phi$	phase fluctuation
$\vec{x}$	arbitrary Cartesian coordinates
s	arc length along unperturbed path
$k(\vec{x})$	unperturbed wavenumber
$D(\vec{x}_1, \vec{x}_2)$	generalized phase-structure function
$D_P(\Delta y)$	transverse acoustic phase-structure function
$D_m(\Delta_y)$	transverse modal phase-structure function
$\Lambda_P(\Delta y)$	logarithmic phase structure $\ln D_p(\Delta y)$
$R_P(\Delta y)$	acoustic pressure coherence
$R_{A_m}(\Delta y)$	acoustic mode coherence
$\tilde{R}_P(\Delta y)$	acoustic phase coherence
$\tilde{R}_{A_m}(\Delta y)$	modal phase coherence
H_m	acoustic mode structure weight

Q_o	acoustic source strength
$\Psi_m(r,\theta;z)$	acoustic mode eigenfunction
$A_m(r,\theta)$	acoustic mode amplitude
$\tilde{A}_m(y)$	mode amplitude phase
$\hat{A}_m$	reduced mode amplitude
$k_m(r,\theta)$	acoustic horizontal wavenumber (eigenvalue)
$\kappa_m(x,y)$	reduced acoustic horizontal wavenumber
$\bar{\kappa}_m$	mean reduced horizontal wavenumber
λ_m	horizontal wavelength of acoustic mode
$u_m(x,y)$	deterministic eigenvalue perturbations
$\mu_m(x,y)$	stochastic eigenvalue perturbations
$v(x,y;z)$	deterministic sound-speed perturbations
$\nu(x,y;z)$	stochastic sound-speed perturbations
ρ_m	two-point correlation of μ_m
$\bar{\rho}$	mean density scale
$\delta\rho$	zero-mean density fluctuation
$\psi_m(x,y)$	parabolic approximation of mode amplitude
l_e	environmental fluctuation scale length
D_p	integration over all paths
$U_m(x,y_p(x))$	deterministic part of path integral
α, β	principal ray labels
$\bar{x}$	mean range
Δ_x	range separation
$y_\alpha(x)$	transverse position of rays
$\Delta_{\alpha\beta}(r)$	transverse separation of rays
Y	transverse position along array
Y_α, Y_β	transverse position of rays at array
Δ_y	transverse separation at array
γ_h	horizontal wavenumber of environmental fluctuations
γ_x,γ_y	Cartesian wavenumbers of environmental fluctuations
$S_m(\gamma_x,\gamma_h)$	environmental fluctuation spectrum
$\partial_a/\partial z$	adiabatic gradient
$\partial_p/\partial z$	potential gradient
f_c	local Coriolis frequency
ω_j	internal-wave frequency
$N(x,y;z)$	buoyancy frequency
$\bar{N}$	depth-averaged buoyancy frequency
$\mathscr{N}_{m,j}(\gamma_h)$	buoyancy-modal interaction integral
$\zeta(x,y;z,t)$	internal-wave displacement
$W_j(x,y;z,\gamma_h)$	internal-wave eigenfunctions
$g_j(\gamma_h,\theta)$	internal-wave spectral amplitude

$G_j(\gamma_h)$	internal-wave power spectra
$\mathscr{I}_{m,j}(\Delta_y)$	internal-wave structure-function integral
$\mathscr{E}$	internal-wave energy per unit area
$E_j(\gamma_h)$	Garrett–Munk spectrum
E_0	Garrett–Munk energy scale
$\tilde{E}_j(\gamma_h)$	normalized Garrett–Munk spectrum
Q_j	internal-wave spectral normalization constant
$\tilde{M}_j$	internal-wave mode energy partition
M	internal-wave mode normalization constant
j_*	Garrett–Munk reference mode
p	Garrett–Munk mode exponent
γ_j	Garrett–Munk spectral peak
$S_j(\omega)$	experimental internal-wave spectrum $\left(\mathrm{m}^2/\left(\mathrm{rad/s}\right)\right)$
$F_j(\gamma_h)$	experimental internal-wave spectrum $\left(\left(\mathrm{J/m}^2\right)/\left(\mathrm{rad/m}\right)\right)$